Intergalactic Medium and 21-cm Astrophysics

Yin-Zhe Ma[1]

School of Chemistry and Physics, University of KwaZulu-Natal, Westville Campus, Private Bag X54001, Durban, 4000, South Africa
NAOC-UKZN Computational Astrophysics Centre (NUCAC), University of KwaZulu-Natal, Durban, 4000, South Africa

August 18, 2018

Abstract

This lecture note contains the introductory material of intergalactic medium, Lyman-α forest, and 21-cm astrophysics. It is suitable for advanced undergraduate and first year graduate students to read and study if he/she wants to enter this research field.

Suggested reading list:

A. Textbook, and Overview of Lyman-α forest and 21-cm astrophysics

A. Loeb & S. R. Furlanetto, *The First Galaxies in the Universe*, Princeton University Press, 2013

A. Loeb, *How Did the First Stars and Galaxies Form?*, Princeton University Press, 2010

S. R. Furlanetto, S. P. Oh, & F. H. Briggs, *Phys. Rept.*, **433**, 181 (2006)

B. Seminal paper on Lyman-α forest

X. Fan et al., *Astron. J.*, **132**, 117 (2006)

C. Theoretical Papers on 21-cm cosmology

M. Sitwell, A. Mesinger, Y.-Z. Ma, & K. Sigurdson, *Mon. Not. Roy. Astron. Soc.*, **438**, 2664 (2014)

A. Hall, C. Bonvin, & A. Challinor, *Phys. Rev. D*, **87**, 064026 (2013)

X. Xu, Y.-Z. Ma, & A. Weltman, *Phys. Rev. D*, **97**, 083504 (2018)

P. Bull, P. G. Ferreira, P. Patel, & M. G. Santos, 2015, The Astrophysical Journal, 803, 21

D. Observational Papers on 21-cm cosmology

D1. EDGES results

J. D. Bowman, A. E. E. Rogers, R. A. Monsalve, T. J. Mozdzen, & N. Mahesh, *Nature*, **555**, 67 (2018)

D2. BINGO forecast

R. Battye, I. Browne, T. Chen, et al. 2016, arXiv:1610.06826

R. A. Battye, et al. 2012, arXiv:1209.1041

[1]Email: ma@ukzn.ac.za

M.-A. Bigot-Sazy, et al., *Mon. Not. Roy. Astron. Soc.*, **454**, 3240 (2015)

D3. FAST forecast

M.-A. Bigot-Sazy, Y.-Z. Ma, R. A. Battye et al. *Frontiers in Radio Astronomy and FAST Early Sciences Symposium 2015*, **502**, 41 (2016)

D4. SKA forecast and science

R. Maartens, et al., 2015, arXiv:1501.04076

S. E. Harper, et al. *Mon. Not. Roy. Astron. Soc.*, **478**, 2416 (2018)

Y.-C. Li, & Y.-Z. Ma, 2017, Physical Review D, 96, 063525

P. Bull, P., et al. 2015, Advancing Astrophysics with the Square Kilometre Array (AASKA14), 24, arXiv: 1501.04088

M. Santos, et al. 2015, Advancing Astrophysics with the Square Kilometre Array (AASKA14), 19, arXiv: 1501.03989

S. Camera, et al. 2015, Advancing Astrophysics with the Square Kilometre Array (AASKA14), 25, arXiv: 1501.03851

L. Wolz, et al. 2015, Advancing Astrophysics with the Square Kilometre Array (AASKA14), 35, arXiv: 1501.03823

A. Raccanelli, 2015, Advancing Astrophysics with the Square Kilometre Array (AASKA14), 31, arXiv: 1501.03821

L. Koopmans, 2015, Advancing Astrophysics with the Square Kilometre Array (AASKA14), 1, arXiv: 1505.07568

S. Colafrancesco, 2015, Advancing Astrophysics with the Square Kilometre Array (AASKA14), 100, arXiv: 1502.03738

D5. PAPER and HERA projects

Please go to `http://reionization.org/science/papers/`, and find the relevant papers.

Contents

1 High-redshift Intergalactic Medium **2**

1.1 Lyman-α Absorption . . . 2

1.1.1 Lyman-α Cross-section . . . 3

1.1.2 Radiative Transfer, Lyman-α optical depth . . . 5

1.1.3 Lyman-α forest . . . 6

1.1.4 Gunn-Peterson trough . . . 7

1.2 21-cm Line . . . 7

1.2.1 Preliminary: Einstein coefficients and emission process . . . 8

1.2.2 Radiative Transfer . . . 12

2 Low-redshift Universe: 21-cm Intensity Mapping **15**

2.1 21-cm Brightness Temperature . . . 15

2.2 Relativistic Perturbation to 21-cm brightness temperature . . . 18

2.2.1 Metric perturbation . . . 19

2.2.2 Orthogonal Frame Vectors . . . 19

2.2.3 Scalar perturbations in conformal Newtonian gauge . . . 19

2.2.4 Brightness temperature fluctuation . . . 22

$n_{\rm HI}$ term. . . . 23

Preparation for calculating $|{\rm d}\lambda/{\rm d}z|$ term. . . . 23

$|{\rm d}\lambda/{\rm d}z|$ term. . . . 24

$(\epsilon_{\rm A}/a(\overline{\eta}_z))$ term. . . . 25

Putting together for $T_{\rm b}(z,\hat{\mathbf{n}})$. . . . 26

2.2.5 Doppler shift . . . 27

2.2.6 Why lensing isn't important at first order? . . . 27

2.2.7 From theory to observables . . . 29

2.2.8 Power spectra and its relative components . . . 33

3 Observational prospects for 21-cm intensity mapping **34**

3.1 BAO reconstruction . . . 34

3.2 Forecasts for BINGO, FAST and SKA . . . 34

3.3 Foreground removal technique . . . 34

3.4 $1/f$ noise . . . 34

A Etherington's Reciprocity relation **34**

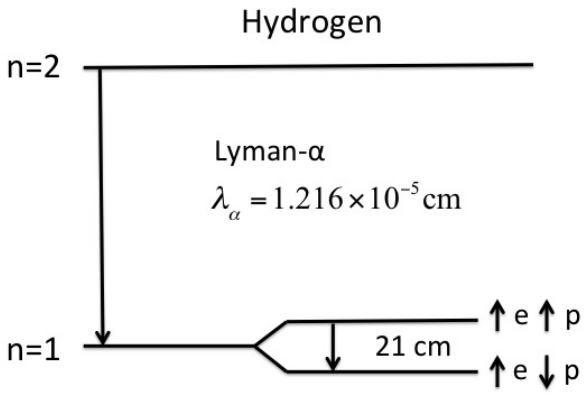

Figure 1: Two important transitions of the hydrogen atom. The Lyman-α transition is the transition in between $n = 2$ and $n = 1$ levels (n is the principal quantum number), and results in the emission of Lyman-α photons with wavelength $\lambda_\alpha = 1.216 \times 10^{-5}$ cm, corresponding to the frequency $\nu_\alpha = 2.468 \times 10^{15}$ Hz. The 21-cm transition occurs between the hyperfine states of the ground energy level ($n = 1$), where the parallel align of the spin in between electron e^- and proton p is on a slightly higher energy state than anti-parallel. The resulted wavelength of transition is 21 cm, corresponding to 1420 MHz.

1 High-redshift Intergalactic Medium

In this section, we will provide an introduction to high-reshift intergalactic medium through the measurement of neutral hydrogen absorption line in the Lyman-α forest system. Then we introduce the 21-cm transition line for the high redshift Universe.

1.1 Lyman-α Absorption

We first study how are the baryons distributed in the Universe inferred from the famous Lyman-α forecast measurement. Hydrogen is the most abundant element in the Universe (the mass fraction is $X_\mathrm{p} \simeq 0.74$, with the rest almost helium $Y_\mathrm{p} \simeq 0.24$.) The predominance of neutral hydrogen is now well-understood by the Big-Bang Nucleo-synthesis (BBN) theory, which effectively combine all neutrons with protons into helium. As a result, the heavier elements are formed inside the stars during the stellar evolution process. We expect more IGM is dominated by hydrogen and helium than Milky Way.

Since the lifetime of hydrogen atom with energy level $n > 1$ is far shorter than the typical time it takes to excite them in the rarefied environment of the Universe, most of the hydrogen is in its ground state (lowest energy level $n = 1$, see Fig. 1), we denote them as HI.

The most widely discussed transition with hydrogen is the Lyman-α spectral line which is transition state of hydrogen from $n = 2$ state to $n = 1$ state. In 1965, Jim Gunn and Bruce Peterson [2] realized that then cross-section of Lyman-α transition is so large that even the neutral

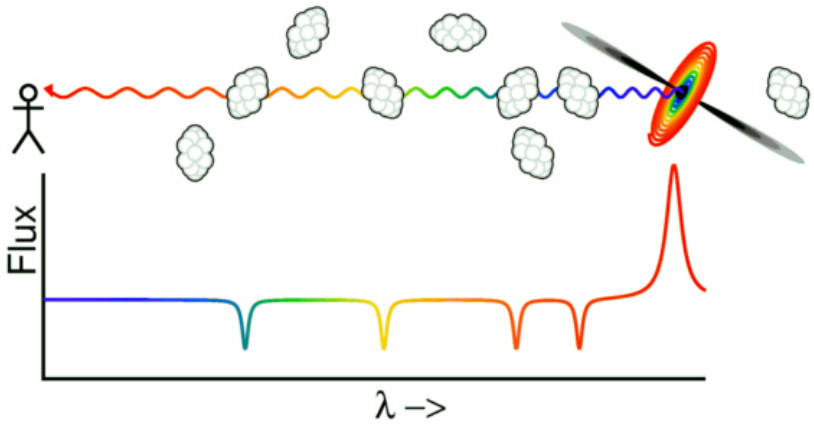

Figure 2: Lyman-α forest. At the top of the panel, the light emitted from the distant quasar passes through several clouds of neutral hydrogen before seen by an observer. The quasar emitted the a high flux of radiation at Lyman-α resonance wavelength. As those photons travel, they are redshifted, so the whole spectrum moves to the right. Photons beginning blue-ward of the Lyman-α transition eventually redshift through that resonance. If the photons are inside the Lyman-α clouds, they will be absorbed by those clouds, producing the absorption features in the spectrum. Therefore the quasar spectrum allows us to map out the column density of IGM neutral hydrogen and ionization structure.

hydrogen fraction is as small as 10^{-5}, the IGM could be looked opaque.

Imagine a photon is emitted at $\lambda < \lambda_\alpha$, where $\lambda_\alpha = 1216$Å. The photon wavelength will be stretched as the Universe expands, and eventually its wavelength is lengthened close to Lyman-α resonance wavelength. Then it could be absorbed by a hydrogen atom and re-emitted in a different direction. We will therefore need to integrate all the way across resonance line to compute the optical depth.

1.1.1 Lyman-α Cross-section

The full cross-section for a single atom is

$$\sigma_\alpha(\nu) = \frac{3\lambda_\alpha^2\Lambda_\alpha^2}{8\pi}\frac{(\nu/\nu_\alpha)^4}{4\pi^2(\nu-\nu_\alpha)^2 + (\Lambda_\alpha^2/4)(\nu/\nu_\alpha)^6}, \tag{1.1}$$

where $\nu_\alpha = (c/\lambda_\alpha) = 2.468\times10^{15}$ Hz is the Lyman-α resonance frequency, $\Lambda_\alpha = 8\pi^2e^2f_\alpha/(3m_ec\lambda_\alpha^2) = 6.25\times10^8\,\mathrm{s}^{-1}$ is the Lyman-α $(2p \to 1s)$ decay rate, $f_\alpha = 0.4162$ is the oscillation strength. This is the formula for classical Rayleigh scattering.

In principal, the thermal velocity of IGM also has a finite spread, but those spread is small comparing to the cosmological redshift, so we safely ignore them.

Since we are mostly interested in absorption close to the resonance, we take the limit of $\nu \to \nu_0$ and write

$$\sigma_\alpha(\nu) = \frac{3\lambda_\alpha^2\Lambda_\alpha}{8\pi}\cdot\left[\frac{1}{\pi}\frac{(\Lambda_\alpha/4\pi)}{(\nu-\nu_\alpha)^2 + (\Lambda_\alpha/4\pi)^2}\right]. \tag{1.2}$$

Since $\nu_\alpha \gg \Lambda_\alpha$, we can use one of the definition of Dirac delta function

$$\delta_\mathrm{D}(x) = \frac{1}{\pi}\lim_{\epsilon\to0}\frac{\epsilon}{x^2+\epsilon^2}, \tag{1.3}$$

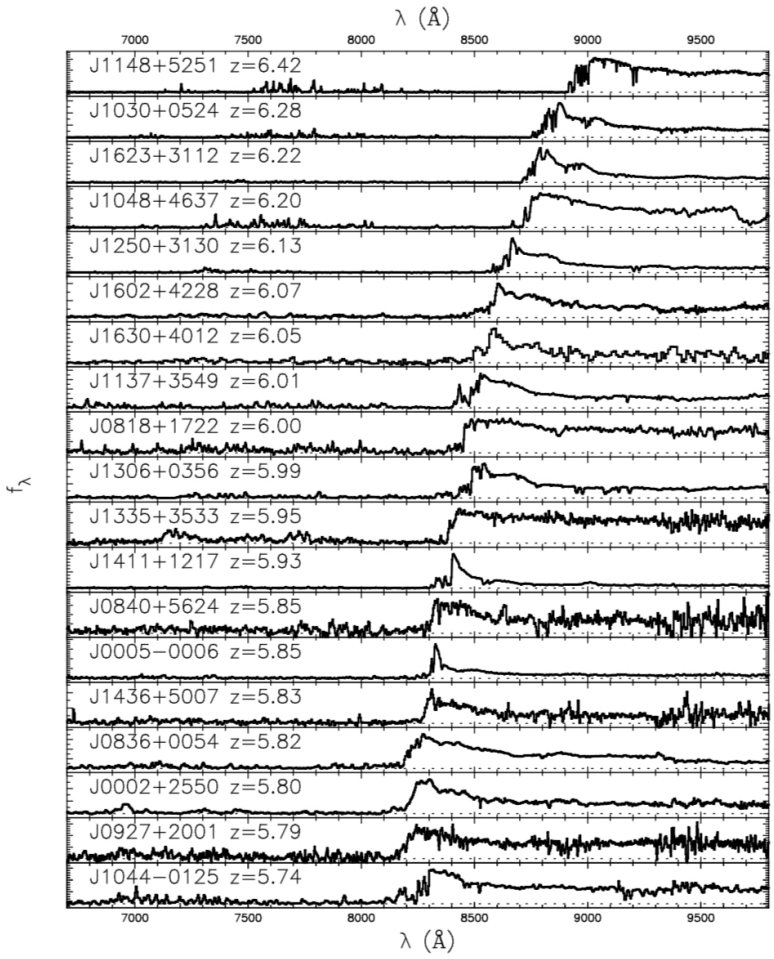

Figure 3: Observations of the 19 quasar spectra from Slogan Digital Sky Survey in between redshift $5.74 < z < 6.42$. For those high-reshift quasars, the spectra show no transmitted flux at the wavelength shortward of the Lyman-α wavelength at the quasar redshift. This is the so-called *Gunn-Peterson* trough which indicates the slight increase of the density of HI in the IGM. Figure taken from [1].

and convert the optical depth to be

$$\begin{aligned}\sigma_\alpha(\nu) &= \frac{3\lambda_\alpha^2\Lambda_\alpha}{8\pi}\delta_{\rm D}(\nu-\nu_\alpha)\\ &= \frac{\pi e^2}{m_{\rm e}c}f_\alpha\delta_{\rm D}(\nu-\nu_\alpha)\\ &\equiv \sigma_0\nu_\alpha\delta_{\rm D}(\nu-\nu_\alpha),\end{aligned} \tag{1.4}$$

where

$$\begin{aligned}\sigma_0 &= \frac{\pi e^2\lambda_\alpha f_\alpha}{m_{\rm e}c^2}\\ &\simeq 4.15\times10^{-18}\,{\rm cm}^2.\end{aligned} \tag{1.5}$$

1.1.2 Radiative Transfer, Lyman-α optical depth

Let us suppose a total flux of light F, transverse a region with size Δl with neutral hydrogen density $n_{\rm HI}$, the flux will lose an amount

$$\Delta F = -F n_{\rm HI}\,\sigma_\alpha\Delta l. \tag{1.6}$$

Integrated it over, we have

$$F^{\rm out} = F_0 e^{-\int n_{\rm HI}\sigma_\alpha {\rm d}l} = F_0 e^{-\tau}, \tag{1.7}$$

where F_0 is the unattenuated flux, and we define the optical depth as an integration along line-of-sight towards us

$$\tau \equiv \int_0^l n_{\rm HI}\,\sigma_\alpha(\nu){\rm d}l, \tag{1.8}$$

where the integral is over the proper length ${\rm d}l$. We need to relate ${\rm d}l$ to ${\rm d}z$ and then ${\rm d}\nu$ to carry out the integral. First we have

$${\rm d}l = c{\rm d}t = c\frac{{\rm d}t}{{\rm d}a}{\rm d}a = \frac{c}{H(z)}\frac{{\rm d}a}{a}. \tag{1.9}$$

Then since $\nu_{\rm obs}/\nu = a$, we have

$$\begin{aligned}\tau &= \int n_{\rm HI}(a)\sigma_\alpha\left(\nu_{\rm obs}/a\right)\frac{c}{H(a)}\frac{{\rm d}a}{a}\\ &= \int n_{\rm HI}(a)\sigma_0\nu_\alpha\delta_{\rm D}\left(\nu_{\rm obs}/a-\nu_\alpha\right)\frac{c}{H(a)}\frac{{\rm d}a}{a}\\ &= n_{\rm HI}(z)\sigma_0\frac{c}{H(z)}\\ &= n_{\rm HI}(z)\sigma_0\frac{c}{H_0}\frac{1}{E(z)},\end{aligned} \tag{1.10}$$

where we have used the fact that $\nu_\alpha/\nu_{\rm obs} = (1+z)$.

Now we can write

$$\begin{aligned} n_{\rm HI}(z) &= \left(\frac{n_{\rm HI}}{n_{\rm H}}\right)\left(\frac{n_{\rm H}}{\bar{n}_{\rm H}}\right)\bar{n}_{\rm H}(z) \\ &= x_{\rm HI}(1+\delta)\left[\frac{X_{\rm p}\Omega_{\rm b}\rho_{\rm cr}(1+z)^3}{m_{\rm p}}\right]. \end{aligned} \tag{1.11}$$

Then we substitute Eq. (1.11) into Eq. (1.10), and use the fact that at high redshift $E(z) = \left[\Omega_{\rm m}(1+z)^3+\Omega_\Lambda\right]^{1/2} \simeq \Omega_{\rm m}^{1/2}(1+z)^{3/2}$, we obtain

$$\tau = 1.6\times10^5\, x_{\rm HI}(1+\delta)\left(\frac{\Omega_{\rm m}h^2}{0.147}\right)^{-1/2}\left(\frac{X_{\rm p}}{0.75}\right)\left(\frac{\Omega_{\rm b}h^2}{0.023}\right)\left(\frac{1+z}{4}\right)^{3/2}, \tag{1.12}$$

which is the well-known *Gunn-Peterson optical depth*. One can see that Lyman-α cloud is very efficient in absorbing photons, and even a small fraction of $x_{\rm HI}$ (e.g. $x_{\rm HI}\sim10^{-5}$) would absorb photons very efficient, producing a large value of optical depth (IGM is opaque). The IGM optical depth can be enormous even if the neutral fraction is small. Any transmission across those wavelength is therefore evidence that the diffuse IGM is highly ionized.

It is possible to use higher order Lyman series lines, see Ref. [3], but you only gain a factor of ~ 20 by going into Lyman-γ and higher order lines are exceedingly hard to measure accurately because they blend with lower redshift Lyman-α absorptions.

1.1.3 Lyman-α forest

In the usual cases, the IGM absorption is observed against a luminous background, such as a bright quasar or bright gamma-ray burst afterglow. The source emitted photons over an extended continuum, which allows us to see absorption features over a range of wavelength. If the source is located at redshift $z_{\rm s}$, then its Lyman-α transition appears at an observed wavelength $\lambda_\alpha(1+z_{\rm s})$. Photons redward of this point will be even stretched to longer wavelength, so they will never enter resonance with Lyman-α line in the IGM (though they might be absorbed by other elements).

Photons blueward of this point eventually redshift into resonance and are absorbed if the gas is not too highly ionized. Each such photon redshifts into resonance at a particular distance from the observer and the source that depends on its initial wavelength: photons emitted blueward of Lyman-α in the source frame travel a great distance before their wavelength redshifted into 1216Å, but those emitted just blueward of it reach the resonance near the source. Therefore, each observed wavelength samples a different point along the line of sight, this is illustrated in Fig. 2.

The resulting *Lyman-α forest* is so named because of the strong variability of these absorption features (Fig. 3). The redward of 1216Å(in the source frame), the quasar continuum is largely unaffected by the IGM, but the blueward of Lyman-α has a highly variable absorption feature that depends on the detailed structure along the line of sight. These features are due to the fact that a line of sight passes through sheets, filaments, voids of the cosmic web, so the optical depth fluctuates.

1.1.4 Gunn-Peterson trough

If a source is observed along the line of sight where the neutral hydrogen fraction is substantial, then *all* photons with wavelength shorter than $\lambda_\alpha(1+z_\mathrm{s})$Åwould redshift to resonance, and are absorbed by the IGM, and re-emitted into the other direction. Eventually this process would result in a *complete* absorption trough blueward of λ_α in the source spectrum, which is known as *Gunn-Peterson trough*.

In Fig. 3, we show the spectra of 19 quasars at redshift $z \sim 6$. The spectra of highest $z \sim 6$ show the hint of Gunn-Peterson effect. However, we cannot use it to infer whether the IGM is highly ionized or not, because as we can see from Eq. (1.12), only a tiny fraction of x_HI can make the optical depth enormous.

The feature of spectral line is that each observational wavelength corresponds to a different distance to us, the other spectral line also has the similar feature.

1.2 21-cm Line

As the powerful tools to study the high redshift Universe, comparing the 21-cm transition, the Lyman-α transitions have the following advantages and disadvantages. The advantages are

- Comparing to 21-cm transition of *spin-flip*, the Lyman-α transition is is several orders of magnitude stronger than this.

The disadvantages are

- The enormous cross-section. The Gunn-Peterson optical depth is so large that even a small neutral hydrogen fraction would end up in an enormous optical depth, making it difficult to study the detail behaviour of hydrogen ionization.
- Since Lyman-α transition lies in the UV band, observing it requires bright UV sources which are rare at high redshifts, limiting the Lyman-α forest study to be only applicable to a limited number of line of sight.
- The high excitation energy of the Lyman-α transition prevents us from using it to study the cold pre-reionization of IGM, because the temperature of IGM before reionization is too low to collisionally excite the Lyman-α line.

To overcome these disadvantages, we can search for a weaker, lower-energy transition of neutral hydrogen, which is the *spin-flip* or hyperfine structure of HI (Fig. 1). So the transition between parallel and anti-parallel state of neutral hydrogen corresponds to the energy which photon's wavelength is 21-cm. The effective optical depth is roughly 1%, which makes the entire neutral IGM accessible during the cosmic dawn.

Figure 4 illustrates the observable effect of 21-cm transition with analogy to Swiss cheese. Each slice of cheese has a different structure, depending on where the air bubbles happen to lie within it. By slicing the Swiss cheese, the full map of distribution of HI as a function of redshift would provide a 3D image of the the Swiss-cheese structure. So the *tomography* of the HI volume provides the only way to map the distribution almost entire Universe's baryonic matter.

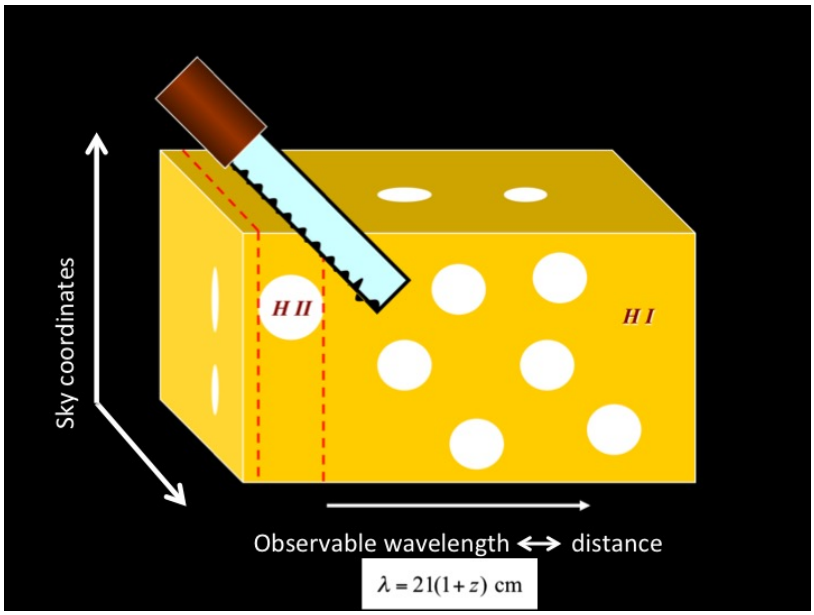

Figure 4: A diagram of 21-cm imaging of ionized bubbles during the epoch of reionization, illustrating to an analogy of slicing Swiss cheese. The two dimensions on each slice is the sky coordinates, and the dimension of slicing is the frequency/wavelength/redshift.

Figure 5 is the cartoon version of the different phases of 21-cm. Figure 6 shows a more concrete and quantitative overview of the evolution of global (sky-averaged) 21-cm brightness temperature relative to the CMB. One can see that the spin-flip background measures the UV and X-ray radiation field over a broad swath of cosmic history, complementing the discrete probes of individual galaxies that are studied by Lyman-α forest.

1.2.1 Preliminary: Einstein coefficients and emission process

In 1916, Albert Einstein proposed that there are three processes occurring in the formation of an atomic spectral line. The three processes are referred to as **spontaneous emission**, **stimulated emission**, and **absorption** (Fig. 8). With each is associated an Einstein coefficient which is a measure of the probability of that particular process occurring. Einstein considered the case of isotropic radiation of frequency ν, and spectral energy density $\rho(\nu)$.

1. **Spontaneous emission** is the process by which an electron "spontaneously" (i.e. without any outside influence) decays from a higher energy level to a lower one (left upper panel of Fig. 8). The process is described by the Einstein coefficient A_{10} (s^{-1}) which gives the probability per unit time that an electron in state 1 with energy E_1 will decay spontaneously to state 0 with energy E_0, emitting a photon with an energy $E_1 - E_0 = h\nu$. If n_i is the number density of atoms in state i, then the change in the number density of atoms in state 1 per unit time due to spontaneous emission will be:

$$\left(\frac{\mathrm{d}n_1}{\mathrm{d}t}\right)_{\mathrm{spon}} = -A_{10}n_1, \tag{1.13}$$

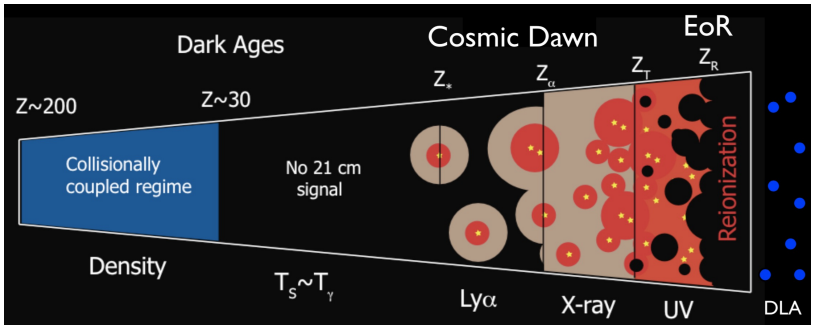

Figure 5: Cartoon of different phases of the 21-cm signal. The signal transitions from the an early phase of collisional coupling to a later phase of Lyman-α coupling through a short period where there is little signal. Fluctuations after this phase are dominated by spatial variation in the Lyman-α , X-ray and ionizing UV backgrounds. After reionization is completed, there is residual signal from neutral hydrogen in the galaxies. Figure taken from [5].

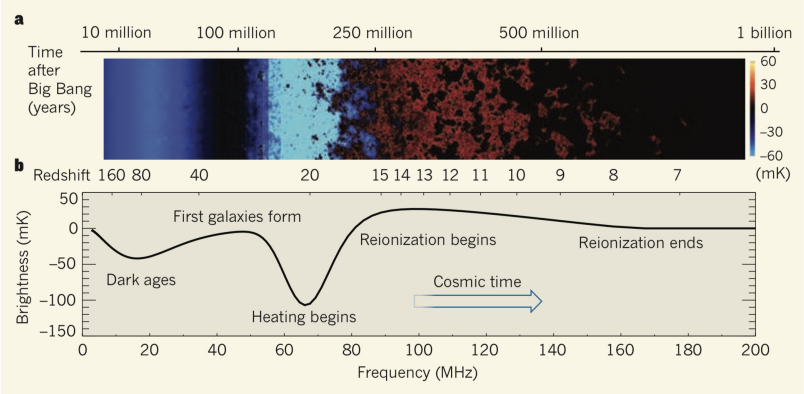

Figure 6: Overview of the global 21-cm signal. *Top panel:* Time evolution of fluctuations in the 21-cm brightness from just before the first stars form to the end of reionization. The colour indicates the strength of the 21-cm brightness as it transits from absorption (blue) to emission (red) and finally disappear (black) due to ionization. *Bottom panel:* Expected evolution of the sky-averaged 21-cm brightness from the dark ages at $z \simeq 150$ to the end of reionization $z \simeq 6$. This process is affected by the interplay of gas heating, the coupling between gas and 21-cm temperatures and ionization of gas. There is a lot of astrophysical uncertainties associated with this process. Figure taken from [6].

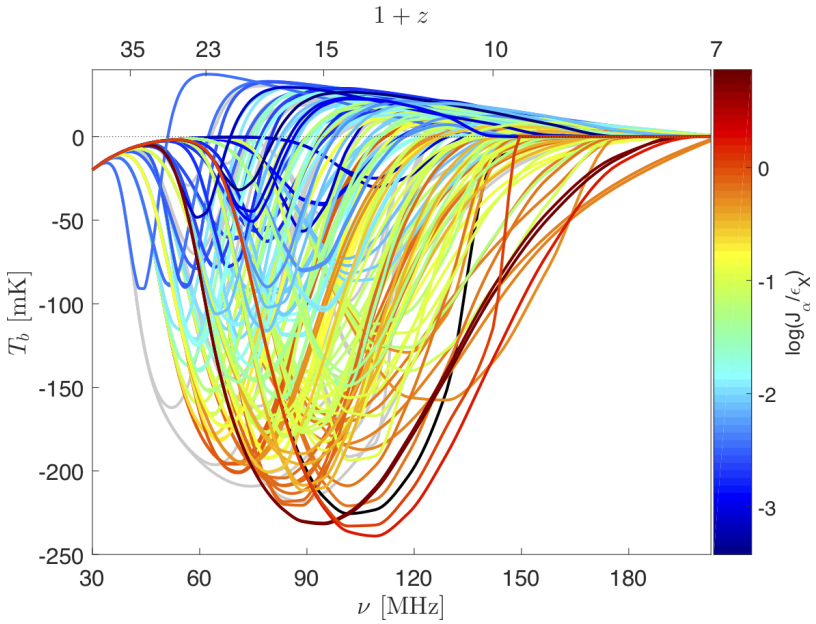

Figure 7: The 21-cm global signal as a function of redshift, for the 193 different astrophysical models, by varying cooling channel, star formation efficiency (f_*), X-ray efficiency of X-ray sources ($f_{\rm X}$), spectral energy distribution of X-ray sources (SED), and the total CMB optical depth (τ). The color (see the color bar on the right) indicates the ratio between the Lyman-α intensity (in units of erg s^{-1} cm^{-2} Hz^{-1} sr^{-1}) and the X-ray heating rate (in units of eV s^{-1} baryon^{-1}) at the minimum point. Figure taken from [4].

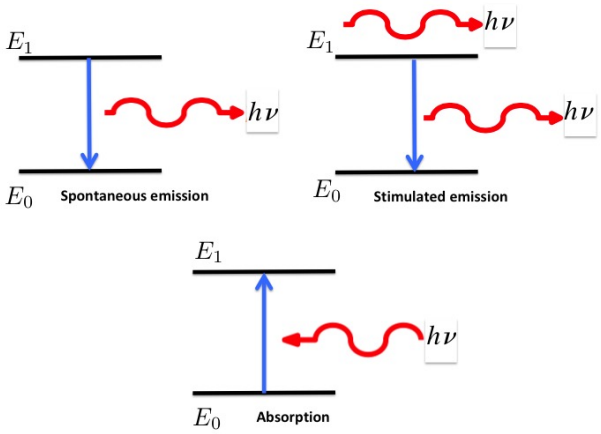

Figure 8: Schematic diagram of atomic spontaneous emission, stimulated emission and absorption.

where the same process results in increasing of the population of the state 0:

$$\left(\frac{\mathrm{d}n_0}{\mathrm{d}t}\right)_{\mathrm{spon}} = A_{10}n_1, \tag{1.14}$$

2. **Stimulated emission** (also known as induced emission) is the process by which an electron is induced to jump from a higher energy level to a lower one by the presence of electromagnetic radiation at (or near) the frequency of the transition (right upper panel of Fig. 8). This process is regarded as negative absorption (or inverse absorption). The process is described by the Einstein coefficient B_{10} ($\mathrm{J}^{-1}\mathrm{m}^3\mathrm{s}^{-2}$), which gives the probability per unit time per unit spectral energy density of the radiation field that an electron in state 1 with energy E_1 will decay to state 0 with energy E_0, emitting a photon with an energy $E_1 - E_0 = h\nu$. The change in the number density of atoms in state 0 per unit time due to induced emission will be:

$$\left(\frac{\mathrm{d}n_0}{\mathrm{d}t}\right)_{\mathrm{stim}} = B_{10}n_1\rho_\nu, \tag{1.15}$$

again, for conservation

$$\left(\frac{\mathrm{d}n_1}{\mathrm{d}t}\right)_{\mathrm{stim}} = -B_{10}n_1\rho_\nu, \tag{1.16}$$

where ρ_ν denotes the spectral energy density of the isotropic radiation field at the frequency of the transition, i.e.

$$\rho_\nu = \frac{8\pi h\nu^3}{c^3}\frac{1}{\mathrm{e}^{h\nu/k_\mathrm{B}T} - 1} \equiv F(\nu)N_\gamma, \tag{1.17}$$

where we have defined $F(\nu) = 8\pi h\nu^3/c^3$ and photon occupation number $N_\gamma = 1/(\exp(h\nu/k_\mathrm{B}T) - 1)$ in the above equation.

3. **Absorption** is the process by which a photon is absorbed by the atom, causing an electron to jump from a lower energy level to a higher one (see lower panel of Fig. 8). The process is described by the Einstein coefficient B_{01} ($\mathrm{J}^{-1}\mathrm{m}^3\mathrm{s}^{-2}$), which gives the probability per unit time per unit spectral energy density of the radiation field that an electron in state 0 with energy E_0 will absorb a photon with an energy $E_1 - E_0 = h\nu$ and jump to state 1 with E_1. The change in the number density of atoms in state 0 per unit time due to absorption will be:

$$\left(\frac{\mathrm{d}n_0}{\mathrm{d}t}\right)_{\mathrm{absor}} = -B_{01}n_0\rho_\nu. \tag{1.18}$$

Note that from the MaxwellBoltzmann distribution we have for the number of excited atomic species i

$$\frac{n_i}{n} = \frac{g_i e^{-E_i/k_\mathrm{B}T}}{Z}, \tag{1.19}$$

where n is the total number density of the atomic species, excited and unexcited, g_i is the degeneracy (also called the multiplicity) of state i, and Z is the partition function.

In the thermodynamic equilibrium, detailed balance (valid only at equilibrium) requires that the change in time of the number of atoms in level 0 (or 1) due to the above three processes be zero, i.e.

$$\left(\frac{\mathrm{d}n_0}{\mathrm{d}t}\right)_{\mathrm{total}} = A_{10}n_1 + B_{10}n_1\rho_\nu - B_{01}n_0\rho_\nu = 0. \tag{1.20}$$

Then we substitute Eq. (1.19) and Eq. (1.17) into the above equation, we can arrive:

$$A_{10}g_1(\mathrm{e}^{h\nu/k_\mathrm{B}T} - 1) + B_{10}g_1F(\nu) = B_{01}g_0F(\nu)\mathrm{e}^{h\nu/k_\mathrm{B}T}. \tag{1.21}$$

This equation must valid at any given temperature, therefore

$$B_{01}g_0 = B_{10}g_1, \tag{1.22}$$

and

$$A_{10}g_1 = B_{10}g_1F(\nu). \tag{1.23}$$

Therefore, we arrive

$$\frac{B_{10}}{B_{01}} = \frac{g_0}{g_1}, \quad \frac{A_{10}}{B_{10}} = F(\nu) = \frac{8\pi h\nu^3}{c^3}. \tag{1.24}$$

For the ground state and first excitation state of 21-cm neutral hydrogen, $g_1/g_0 = 3$, i.e. $B_{10}/B_{01} = 1/3$.

Therefore, if we count all three processes, in the frame of the gas, the net change in the number of photons per unit volume with energy in between E and $E + \mathrm{d}E$ propagating within a solid angle $\mathrm{d}\Omega$ in proper time $\mathrm{d}t$ is

$$\mathrm{d}n_{\mathrm{emit}} = \frac{\mathrm{d}\Omega}{4\pi}\left[A_{10}n_1 + B_{10}n_1\rho_\nu - B_{01}n_0\rho_\nu\right]\mathrm{d}t\mathrm{d}E\delta(E - E_{21}), \tag{1.25}$$

then we substitute Eqs. (1.24) and (1.17) into the above equation and simplify, one can reach

$$\mathrm{d}n_{\mathrm{emit}} = \frac{1}{4\pi}A_{10}\left[n_1 + (n_1 - 3n_0)N_\gamma\right]\mathrm{d}t\mathrm{d}E\delta(E - E_{21})\mathrm{d}\Omega, \tag{1.26}$$

which is Eq. (2.1).

1.2.2 Radiative Transfer

More radiative transfer to be added in.

The brightness temperature of 21-cm can be written as

$$\begin{aligned}\delta T_\mathrm{b}(\nu) = &\quad \frac{T_\mathrm{s} - T_\gamma}{1+z}(1 - e^{-\tau_{\nu_0}}) \\ \approx &\quad 27x_{\mathrm{HI}}(1+\delta_\mathrm{b})\left(\frac{H}{\mathrm{d}v_\mathrm{r}/\mathrm{d}r + H}\right)\left(1 - \frac{T_\mathrm{cmb}}{T_\mathrm{s}}\right)\left(\frac{1+z}{10}\frac{0.15}{\Omega_\mathrm{m}h^2}\right)^{1/2}\left(\frac{\Omega_\mathrm{b}h^2}{0.023}\right)\mathrm{mK},\end{aligned} \tag{1.27}$$

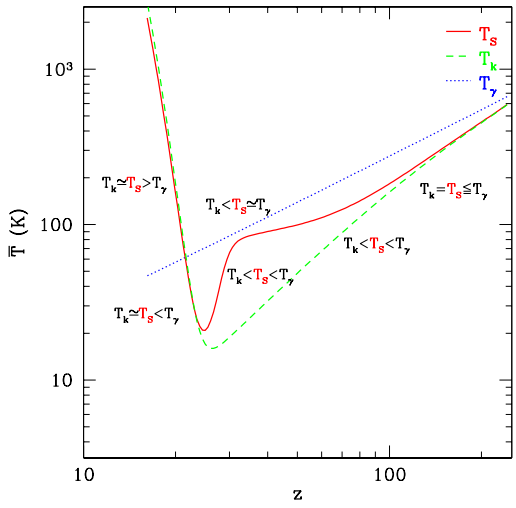

Figure 9: Evolution of spin temperature $T_{\rm s}$, gas temperature T_K and CMB temperature T_γ. This figure is taken from [11].

where $T_{\rm s}$ is the gas spin temperature, τ_{ν_0} is the optical depth at the 21-cm frequency ν_0, $\delta_{\rm b}(\mathbf{x}, z) \equiv \rho/\bar{\rho} - 1$ is the evolved (Eulerian) density contrast of baryons, $H(z)$ is the Hubble parameter, $\mathrm{d}v_{\rm r}/\mathrm{d}r$ is the comoving gradient of the line of sight component of the comoving velocity, and all quantities are evaluated at redshift $z = \nu_0/\nu - 1$. Therefore the brightness temperature of 21-cm is very sensitive to the spin temperature of gas and CMB temperature [11]. In addition, we have marked the factors that are related to cosmology as red, and factors that are astrophysical determined as blue. Once can see the rich dependence of astrophysics and cosmology for this global brightness temperature.

1. **Collisional coupling;** $\bar{T}_{\rm k} = \bar{T}_{\rm s} \leq T_{\rm cmb}$: At high redshifts, the IGM is dense, so the spin temperature is collisionally coupled to the gas kinetic temperature. The gas temperature is originally coupled to the CMB, but after decoupling cools adiabatically as $\propto (1+z)^{-2}$, faster than the CMB. The 21-cm brightness temperature offset from the CMB in this regime starts at zero, when all three temperatures are equal, and then becomes increasingly negative as $T_{\rm s}$ and $T_{\rm k}$ diverge more and more from $T_{\rm cmb}$. The fluctuations in $\delta T_{\rm b}$ are driven by the density field, as collisional coupling is efficient everywhere In the fiducial model, this corresponds to $z \gtrsim 100$.

2. **Collisional decoupling;** $\bar{T}_{\rm k} < \bar{T}_{\rm s} < T_\gamma$: The IGM becomes less dense as the Universe expands. The spin temperature starts to decouple from the kinetic temperature, and begins to approach the CMB temperature again, thus $\delta T_{\rm b}$ starts rising towards zero. Decoupling from $T_{\rm k}$ occurs as a function of the local gas density, with underdense regions decoupling first. The power spectrum initially steepens, as small-scale density fluctuations drive the additional fluctuations of the collisional coupling coefficient. As the spin temperature in even the overdense regions finally decouples from the kinetic temperature, the power spec-

trum flattens again, and the mean signal drops as $\bar{T}_{\rm s} \to 0$. In the fiducial model, this epoch corresponds to $35 \lesssim z \lesssim 100$.

3. **Collisional decoupling → WF coupling transition;** $\bar{T}_{\rm k} < \bar{T}_{\rm s} \approx T_\gamma$: As the spin temperature throughout the IGM decouples from the kinetic temperature, the mean signal is faint and might disappear, if the first sources wait long enough to ignite. In the fiducial model, this transition regime doesn't really exist. In fact our first sources turn on before the spin temperature fully decouples from the kinetic temperature.

4. **WF coupling;** $\bar{T}_{\rm k} < \bar{T}_{\rm s} < T_\gamma$: The first astrophysical sources turn on, and begin coupling the spin temperature of the nearby IGM to the kinetic temperature through the WF effect (Lyα coupling), i.e. the UV resonant scattering couples $T_{\rm s}$ to $T_{\rm k}$. As the requirements for Lyα coupling are more modest than those to heat the gas through X-ray heating, the kinetic temperature keeps decreasing in this epoch. The mean brightness temperature offset from the CMB starts becoming more negative again and can even reach values of $\delta T_{\rm b} < -100$ mK. In the fiducial model, this epoch corresponds to $25 \lesssim z \lesssim 35$.

5. **WF coupling → X-ray heating transition;** $\bar{T}_{\rm k} \sim \bar{T}_{\rm s} < T_\gamma$: Lyα coupling begins to saturate as most of the IGM has a spin temperature which is strongly coupled to the kinetic temperature. The mean spin temperature reaches a minimum value, and then begins increasing. A few underdense voids are left only weakly coupled as X-rays from the first sources begin heating the surrounding gas in earnest, raising its kinetic temperature. The 21-cm power spectrum steepens dramatically as small-scale overdensities now host hot gas, while on large scales the gas is uniformly cold as Lyα coupling saturates. As inhomogeneous X-ray heating continues, the large-scale power comes back up. In our fiducial model, this transition occurs around $z \sim 25$.

6. **X-ray heating;** $\bar{T}_{\rm k} = \bar{T}_{\rm s} < T_\gamma$: X-rays start permeating the IGM. The fluctuations in $\delta T_{\rm b}$ are now at their maximum, as regions close to X-ray sources are heated above the CMB temperature, $\delta T_{\rm b} > 0$, while regions far away from sources are still very cold, $\delta T_{\rm b} < 0$. A "shoulder" in the power spectrum, similar to that seen in the epoch of reionization, moves from small scales to large scales. X-rays eventually heat the entire IGM, and 21-cm can only be seen in emission. The power spectrum falls as this process nears completion. In our fiducial mode, this epoch corresponds to $18 \lesssim z \lesssim 25$.

7. **X-ray heating → reionization transition;** $\bar{T}_{\rm k} = \bar{T}_{\rm s} > T_\gamma$: X-rays have heated all of the IGM to temperatures above the CMB. The 21-cm signal becomes insensitive to the spin temperature. Emission in 21-cm is now at its strongest before reionization begins in earnest. The 21-cm power spectrum is driven by the fluctuations in the density field. In our fiducial model, this epoch corresponds to $16 \lesssim z \lesssim 18$.

8. **Reionization** : Ionizing photons from early generations of sources begin permeating the Universe, wiping-out the 21-cm signal inside ionized regions. The power spectrum initially drops on large scales at $\bar{x}_{\rm HI} \gtrsim 0.9$ as the first regions to be ionized are the small-scale overdensities. The mean signal decreases as HII regions grow, and the power spectrum is

governed by HII morphology. This epoch can have other interesting features depending on the detailed evolution of the sources and sinks of ionizing photons, as well as feedback processes, but as the focus of this section is the pre-reionization regime, we shall be brief in this point. In our fiducial model, this epoch corresponds to $7 \lesssim z \lesssim 16$. So eventually all gases have been ionized and there is no source to provide kinetic temperature, the $T_{\rm s}$ comes back to $T_{\rm CMB}$.

The reason that step 6 is later than step 4 is because the X-rays is only emitted when the violent astrophysics starts to happen inside the galaxies, so it takes some time for structure to form. It also takes some time for emitted X-rays to be absorbed by the HI.

The late time 21-cm intensity mapping signal comes out of the HI synthesized during structure evolution.

2 Low-redshift Universe: 21-cm Intensity Mapping

In the following calculation we take $c = 1$, and metric convention $(+, -, -, -)$.

2.1 21-cm Brightness Temperature

Much of the following materials are presented in [8], but here we present a more detail calculation through each step. Let the rest-frame (proper) number density of neutral hydrogen atoms at redshift z along some line-of-sight be $n_{\rm HI}$, with a fraction $n_1/n_{\rm HI}$ being in the excited states and $n_0/n_{\rm HI}$ in the singlet state of the 21-cm hyperfine transition. One should notice that the excited state has $S = 1$ thus it has three degenerated state $2S + 1$. Therefore, the net change in the number of photons per volume with energy between E and $E + {\rm d}E$ propagation within a solid angle ${\rm d}\Omega$ in proper time ${\rm d}t$ due to 21-cm transition is

$$ {\rm d}n_{\rm emit} = \frac{1}{4\pi} \left[(n_1 - 3n_0) N_\gamma + n_1 \right] A_{10} \delta(E - E_{21}) {\rm d}E {\rm d}t {\rm d}\Omega, \tag{2.1} $$

where $A_{10} \simeq 2.869 \times 10^{-15} {\rm s}^{-1}$ is the spontaneous emission coefficient, and $E_{21} = 5.88 \mu{\rm eV}$ is the rest-frame energy of 21-cm photon. N_γ is the photon occupation number, and in the Black-body case, it is in the Planck form $N_\gamma = \left({\rm e}^{h\nu/k_{\rm B}T_{\rm rad}} - 1 \right)^{-1} = \left({\rm e}^{T_{21}/T} - 1 \right)^{-1}$. The first term $(n_1 N_\gamma)$ is the stimulated emission, where the incident photons causing the first excited state to emit a photon and jumps into ground state, and it also has the inverted process where the ground state atom absorbs a photon and jumps up to the first excited state. The second term $-3n_0 N_\gamma$ is the absorption term which corresponds to the case where a ground state atom absorbs photon and jumps onto first excitation state. The third term n_1 is just the spontaneous emission from $1 \to 0$. One can verify that, in case of thermal equilibrium $(n_1/n_0 = 3{\rm e}^{-T_{21}/T})$ the square bracket in Eq. (2.1) is equal to zero, i.e. no emission at all. The detail derivation is shown in Appendix 1.2.1.

The level of population defined by the spin temperature $T_{\rm s}$ by $n_1/n_0 = 3{\rm e}^{-T_{21}/T_{\rm s}}$, where $T_{21} \equiv E_{21}/k_{\rm B} = 0.068{\rm K}$. We assume that the radiation field consists of CMB and addition 21-cm photons. At low redshift $T_{\rm K} \simeq T_{\rm s} \gg T_{\rm CMB} \gg T_{21}$. In this limit, $n_1 \simeq 3n_0$, therefore

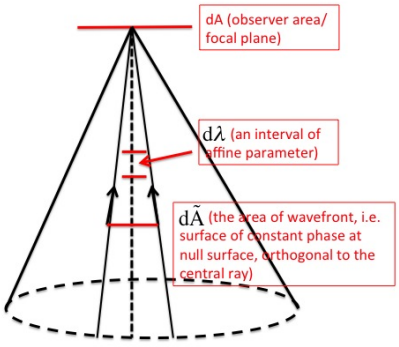

Figure 10: The congruence of the light-ray bundles, the area of wavefront and the observer's focal plane.

$n_{\rm HI} = (4/3)n_1$. Equation (2.1) becomes

$$\mathrm{d}n_{\rm emit} \simeq \frac{3}{16\pi} n_{\rm HI}\, A_{10}\delta(E - E_{21})\mathrm{d}E\mathrm{d}t\mathrm{d}\Omega, \tag{2.2}$$

which is independent of spin temperature. Note that $\mathrm{d}n_{\rm emit}$ defined by Eqs. (2.1) and (2.2) have the dimension of number density.

The number of photons collected by an observer with 4-velocity u^a along the line-of-sight $\hat{\mathbf{n}}$, with energies between E and $E + \mathrm{d}E$ in an area $\mathrm{d}A$ subtending a solid angle at the observer of $\mathrm{d}\Omega$ in a proper time $\mathrm{d}t$ is

$$\mathrm{d}n_{\rm rec} = f(E, \hat{n})E^2\mathrm{d}E\mathrm{d}\Omega\mathrm{d}A\mathrm{d}t, \tag{2.3}$$

note that because photon distribution function $f(E, \hat{n})$ has the unit of $1/h_{\rm p}^3$, the $\mathrm{d}n_{\rm rec}$ is dimensionless. Therefore, in order to relate $\mathrm{d}n_{\rm emit}$ and $\mathrm{d}n_{\rm rec}$, we need to multiply a $\mathrm{d}V$ factor onto $\mathrm{d}n_{\rm emit}$.

We relate the $\mathrm{d}n_{\rm rec}$ and $\mathrm{d}n_{\rm emit}$ by considering the propagation of the bundle of null geodesics that focus on the observer. Referring to Fig. 10, one can see that $\mathrm{d}\tilde{A}$ is the invariant[2] area of the wavefront, i.e. the surface of the constant phase at null surface, orthogonal to the central ray. So $\mathrm{d}\tilde{A}$ is the observer's area at given point x^a. $k^a = \mathrm{d}x^a/\mathrm{d}\lambda$ is the wave vector and x^a is the spacetime position along the light ray. In an interval of affine parameter $\mathrm{d}\lambda$, the wave-front sweeps a volume $\mathrm{d}\tilde{A}u_{\rm s}^a k_a \mathrm{d}\lambda$, where $u_{\rm s}^a$ is the source 4-velocity. Note that the volume is observer-dependent, and $\mathrm{d}\tilde{A}\mathrm{d}x_a = \mathrm{d}\tilde{A}k_a\mathrm{d}\lambda$ is the volume at each position of the beam, and $\mathrm{d}\tilde{A}u_{\rm s}^a k_a\mathrm{d}\lambda$ is the volume projected onto the source system, i.e. volume measured by the source. One can easily see this recovers the ordinary volume in Minkowski spacetime, because in Minkowski spacetime, if the source is at rest, $u_{\rm s}^a = (1, 0, 0, 0)$. This is because the $u_{\rm S}^a$ is just the tangential vector along the source worldline, i.e.

$$u_{\rm S}^a = \left(\frac{\partial}{\partial\tau}\right)_{\rm S}^a = \left(\frac{\partial}{\partial t}\right)^a \left(\frac{\mathrm{d}t}{\mathrm{d}\tau}\right) + \left(\frac{\partial}{\partial x^i}\right)^a \left(\frac{\mathrm{d}x^i}{\mathrm{d}\tau}\right), \tag{2.4}$$

[2] $\mathrm{d}\tilde{A}$ is invariant under Lorentz transformation, independent of local observer, because $\mathrm{d}\tilde{A} = \det\mathcal{D}_{\rm o}\mathrm{d}\Omega_{\rm o}$.

where the second term is zero because of at rest. Thus,

$$\mathrm{d}\tilde{A}u_{\rm s}^a k_a \mathrm{d}\lambda = \mathrm{d}\tilde{A}\left(\frac{\mathrm{d}t}{\mathrm{d}\lambda}\right)\mathrm{d}\lambda = \mathrm{d}\tilde{A}\mathrm{d}t = \mathrm{d}V. \tag{2.5}$$

Now we can relate Eq. (2.2) with Eq. (2.3), we first multiply with the volume (remember the dimension is different between the two, $\mathrm{d}V$ is the local volume, and $\mathrm{d}n_{\rm emit}$ is the photons emitted per volume), and note that Eq. (2.2) is about everything from the emission point

$$\begin{aligned}\mathrm{d}n_{\rm rec} &= \int \mathrm{d}V \mathrm{d}n_{\rm emit} \\ &= \int (\mathrm{d}\tilde{A}k_a u_{\rm s}^a \mathrm{d}\lambda)\left(\frac{3}{16\pi}\right) n_{\rm HI}\, A_{10}\delta(E_{\rm e}-E_{21})\mathrm{d}E_{\rm e}\mathrm{d}t_{\rm e}\mathrm{d}\tilde{\Omega},\end{aligned} \tag{2.6}$$

where $E_{\rm e}$ is the emitted energy, which is related to the measured energy (redshifted energy) E by $E_{\rm e} = E(1+z)$. $\mathrm{d}t_{\rm e}$ is the increment of time at the source, which is related with the time measured by observer at $z=0$ with $\mathrm{d}t_{\rm e} = \mathrm{d}t/(1+z)$. $\mathrm{d}\tilde{\Omega}$ is the solid angle of the observer's area (focal plane) $\mathrm{d}A$ measured from the source. Now we substitute these relations into Eq. (2.6), we have

$$\mathrm{d}n_{\rm rec} = \frac{3}{16\pi}\int \mathrm{d}\lambda \left[n_{\rm HI}\, A_{10}\delta\left(E(1+z)-E_{21}\right)\times \mathrm{d}E(1+z)\frac{\mathrm{d}t}{1+z}k_a u_{\rm s}^a \mathrm{d}\tilde{\Omega}\mathrm{d}\tilde{A}\right]. \tag{2.7}$$

We now use the relation $\mathrm{d}\lambda = |\mathrm{d}\lambda/\mathrm{d}z|\mathrm{d}z$, and the following Dirac-delta function property

$$\delta(E(1+z)-E_{21}) = \frac{\delta\left(z-\frac{E_{21}-E}{E}\right)}{E}, \tag{2.8}$$

and $k_a u_{\rm s}^a = E_{21}$ (energy of the photon measured from the source) and $E_{21}/E = 1+z$ to simplify the above equation. Then Eq. (2.7) becomes

$$\mathrm{d}n_{\rm rec} = \frac{3}{16\pi} n_{\rm HI}\, A_{10}(1+z)\left|\frac{\mathrm{d}\lambda}{\mathrm{d}z}\right|\mathrm{d}E\mathrm{d}t\mathrm{d}\tilde{\Omega}\mathrm{d}\tilde{A}. \tag{2.9}$$

Now we use the *reciprocity relation* (Sec. A) $\mathrm{d}\tilde{A}\mathrm{d}\tilde{\Omega} = \mathrm{d}A\mathrm{d}\Omega/(1+z)^2$, and again $E_{21}/E = 1+z$, to combine Eq. (2.9) with Eq. (2.3), and we obtain

$$f(E,\hat{n}) = \frac{3}{16\pi}\frac{n_{\rm HI}\, A_{10}(1+z)}{E_{21}^2}\left|\frac{\mathrm{d}\lambda}{\mathrm{d}z}\right|. \tag{2.10}$$

In Rayleigh-Jeans regime, $k_{\rm B}T_{\rm b} = h_{\rm p}^3 Ef/2$, where $h_{\rm p}$ is Planck constant [3]. It follows that

$$T_{\rm b}(z,\hat{n}) = \frac{3}{32\pi}\frac{h_{\rm p}^3 n_{\rm HI}\, A_{10}}{k_{\rm B}E_{21}}\left|\frac{\mathrm{d}\lambda}{\mathrm{d}z}\right|. \tag{2.11}$$

Now if we only consider FRW universe, i.e. ignoring perturbation, then the affine parameter λ can be arbitrarily re-scaled, but it needs to be fixed at the source since $k_a u_{\rm s}^a = E_{21}$. Note

[3] This is because $f(\mathbf{x},\mathbf{p}) = \frac{2/h_{\rm p}^3}{\exp(E/(k_{\rm B}T_{\rm b}))-1}$, where $h_{\rm p}^3$ is to make sure $\int f\mathrm{d}^3\mathbf{x}\mathrm{d}^3\mathbf{p}$ is dimensionless, and factor of 2 is due to that photon has two polarization state. In Rayleigh-Jeans regime, $\exp(x)\simeq 1+x$ so one can obtain the equation in the text.

that $|\mathrm{d}\lambda/\mathrm{d}z|$ in Eq. (2.11) is at emission point, and each 21-cm emission has fixed energy E_{21}, therefore

$$\begin{aligned}\left|\frac{\mathrm{d}z}{\mathrm{d}\lambda}\right|_{\rm e} &= \left|\frac{\mathrm{d}}{\mathrm{d}\lambda}\left(\frac{1}{a}\right)\right| = \left|-\frac{\dot{a}}{a^2}\frac{\mathrm{d}\eta}{\mathrm{d}\lambda}\right| = \left|\frac{\mathcal{H}}{a}\frac{\mathrm{d}\eta}{\mathrm{d}\lambda}\right| = H\left|\frac{\mathrm{d}\eta}{\mathrm{d}\lambda}\right|_{\rm e} \\ &= H\left(\frac{\epsilon}{a^2}\right)_{\rm e} = H\left(\frac{E}{a}\right)_{\rm e} = H(1+z)E_{21}, \end{aligned} \tag{2.12}$$

where at the second line we have used the definition of photon 4-momentum, i.e. Eq. (2.31) with $\psi = 0$.

Now we substitute Eq. (2.12) into Eq. (2.11) and adding on c^3 to make correct the dimension to be in temperature, we have

$$\overline{T}_{\rm b}(z) = \left(\frac{3}{32\pi}\right)\frac{(h_{\rm p}c)^3\overline{n}_{\rm HI}A_{10}}{k_{\rm B}E_{21}^2(1+z)H(z)}. \tag{2.13}$$

We then use

$$\overline{n}_{\rm HI} = \overline{n}_{\rm HI}(z) = \frac{\Omega_{\rm HI}(z)\rho_{\rm c}(0)}{m_{\rm p}}\frac{1}{a^3} = \frac{\Omega_{\rm HI}(z)\rho_{\rm c}(0)}{m_{\rm p}}(1+z)^3, \tag{2.14}$$

where $\Omega_{\rm HI}(z)$ is the comoving mass density in HI in unit of current critical density. By substituting Eq. (2.14) into Eq. (2.13), we obtain

$$\begin{aligned}\overline{T}_{\rm b}(z) &= 0.188{\rm K}\left(\Omega_{\rm HI}(z)h\right)\frac{(1+z)^2}{E(z)} \\ &= 0.127\left(\frac{h}{0.7}\right)\left(\frac{\Omega_{\rm HI}(z)}{10^{-3}}\right)\left(\frac{(1+z)^2}{E(z)}\right){\rm mK}, \end{aligned} \tag{2.15}$$

which is clear of its cosmological parameter dependence. For the most general case where curvature is non-zero and dynamical dark energy,

$$E(z) = \left[\Omega_{\rm m}(1+z)^3 + \Omega_{\rm k}(1+z)^2 + \Omega_{\rm de}(1+z)^{3(1+w_0+w_a)}{\rm e}^{-3w_a z/(1+z)}\right]^{1/2}, \tag{2.16}$$

where $\Omega_{\rm m} + \Omega_{\rm k} + \Omega_{\rm de} = 1$ [7]. The above z dependence on dark energy is because, for CPL parametrization, $w(a) = w_0 + w_a(1-a)$,

$$\rho_{\rm de}(a) = \rho_{\rm de0}a^{-3(1+w_0+w_a)}{\rm e}^{3w_a(a-1)}. \tag{2.17}$$

2.2 Relativistic Perturbation to 21-cm brightness temperature

The above Eqs. (2.13) and (2.15) are for the average brightness of 21-cm emission. Now we want to calculate the perturbation of the brightness temperature so that we can do power spectrum estimation and cross-correlation studies.

2.2.1 Metric perturbation

In the following we only consider the the spacetime metric with sign $(+,-,-,-)$. The most general perturbation to the background metric is

$$ds^2 = a^2(\eta)\left((1+2\psi)d\eta^2 - 2B_i dx^i d\eta - [(1-2\phi)\delta_{ij} + 2E_{ij}]\, dx^i dx^j\right), \tag{2.18}$$

where the coordinate transformation is like

$$x^i \to x'^i,\ B_i \to \frac{\partial x^j}{\partial x'^i} B_j,\ E_{ij} \to \frac{\partial x^k}{\partial x'^i}\frac{\partial x^l}{\partial x'^j} E_{kl}, \tag{2.19}$$

and E_{ij} is a symmetric ($E_{ij} = E_{ji}$) and trace-free ($\delta^{ij}E_{ij} = 0$) three-tensor.

2.2.2 Orthogonal Frame Vectors

It is very useful to construct explicitly an *orthonormal frame* of 4-vectors, $(E_0)^\mu$ and $(E_i)^\mu$, in the perturbed metric (the upper index μ is known as *Penrose Abstract Index*). Taken the timelike $(E_0)^\mu$ to be the 4-velocity u^μ of an observer at rest relative to the coordinate system. It follows that $(E_0)^\mu$ must be parallel to δ_0^μ and normalizing gives, at linear order

$$(E_0)^\mu = a^{-1}(1-\psi)\delta_0^\mu, \tag{2.20}$$

since then

$$g_{\mu\nu}(E_0)^\mu(E_0)^\nu = a^{-2}(1-2\psi)g_{00} = a^{-2}(1-2\psi)a^2(1+2\psi) = 1, \tag{2.21}$$

where we have dropped the second order (and above) term here.

The spacelike $(E_i)^\mu$ is a little more involved, since the coordinate vectors δ_i^μ are not orthogonal to u^μ unless $B_i = 0$. The following construction has the required property

$$(E_i)^\mu = a^{-1}\left[B_i\delta_0^\mu + (1+\phi)\delta_0^\mu - E_i^j\delta_j^\mu\right], \tag{2.22}$$

one can easily verify the following two properties at the first order

$$\begin{aligned} g_{\mu\nu}(E_0)^\mu(E_i)^\nu &= 0, \text{Orthogonality} \\ g_{\mu\nu}(E_i)^\mu(E_j)^\nu &= -\delta_{ij}, \text{Normalization.} \end{aligned} \tag{2.23}$$

2.2.3 Scalar perturbations in conformal Newtonian gauge

We only consider scalar perturbation here, and we can also choose two gauge functions so that metric perturbation E and B are zero. This defines *conformal Newtonian gauge*

$$ds^2 = a^2(\eta)\left[(1+2\psi)d\eta^2 - (1-2\phi)\delta_{ij}dx^i dx^j\right], \tag{2.24}$$

In this gauge, the physics appears to be simple because the hypersurfaces of constant time are orthogonal to the worldlines of observers at rest in the coordinate ($g_{0i} = B_i = 0$), and the induced geometry of the constant-time hypersurface is isotropic.

To derive the particle geodesic equation, we first derive the Christoffel symbol. Generally

$$\Gamma^{\mu}_{\nu\rho} = \frac{1}{2} g^{\mu\kappa} \left(\partial_\nu g_{\kappa\rho} + \partial_\rho g_{\kappa\nu} - \partial_\kappa g_{\nu\rho} \right), \tag{2.25}$$

and the metric is diagonal and simple to invert:

$$g^{\mu\nu} = \frac{1}{a^2} \begin{pmatrix} 1-2\psi & 0 \\ 0 & -(1+2\phi)\delta^{ij} \end{pmatrix}. \tag{2.26}$$

Then we can work out the all of the nonzero Christoffel symbols (the dot is referring to the derivative to η)

$$\begin{aligned}
\Gamma^0_{00} &= \mathcal{H} + \dot{\psi} \\
\Gamma^0_{0i} &= \partial_i \psi \\
\Gamma^i_{00} &= \delta^{ij} \partial_j \phi \\
\Gamma^0_{ij} &= \mathcal{H}\delta_{ij} - \left[\dot{\phi} + 2\mathcal{H}(\phi + \psi) \right] \delta_{ij} \\
\Gamma^i_{j0} &= (\mathcal{H} - \dot{\phi})\delta^i_j \\
\Gamma^i_{jk} &= -2\delta^i_{(j}\partial_{k)}\phi + \delta_{jk}\delta^{il}\partial_l \phi,
\end{aligned} \tag{2.27}$$

where the round bracket in the last line means $A_{(ij)} = (1/2)(A_{ij} + A_{ji})$. In addition, all of the over-dot means the partial derivative with respective to conformal time η, i.e. $\dot{()} = \partial_\eta$.

The metric perturbation leads to changes in a photon's energy during propagation relative to the change in an unperturbed cosmology. This effect, in turn, leads to the 21-cm fluctuations (CMB anisotropy is the same reason) on the sky. We shall do the perturbation calculation in conformal Newtonian gauge. We parameterise the photon 4-momentum in terms of the energy E seen by an observer at rest in the coordinates, and by the direction cosines e^i of the propagation direction seen by the same observer on the $(E_i)^\mu$ orthogonal frame of vectors (Eqs. (2.20) and (2.22)). Note that $\delta_{ij}e^i e^j = 1$, the photon 4-momentum is

$$\begin{aligned}
p^\mu &= E\left[(E_0)^\mu + e^i (E_i)^\mu \right] \\
&= Ea^{-1}\left[(1-\psi)\delta^\mu_0 + e^i(1+\phi)\delta^\mu_i \right].
\end{aligned} \tag{2.28}$$

Using the 3-vector notation, and identifying e^i with vector $\mathbf{e}$, we can write

$$\begin{aligned}
p^\mu &= Ea^{-1}\left[(1-\psi), (1+\phi)\mathbf{e} \right] \\
&= \epsilon a^{-2}\left[(1-\psi), (1+\phi)\mathbf{e} \right],
\end{aligned} \tag{2.29}$$

where we have introduced comoving energy $\epsilon \equiv Ea$ which is a constant in the background.

Photons move on geodesic of the perturbed metric so

$$\frac{\mathrm{d}p^\mu}{\mathrm{d}\lambda} + \Gamma^\mu_{\nu\rho} p^\nu p^\rho = 0, \tag{2.30}$$

where λ is an *affine parameter* such that $p^\mu = \mathrm{d}x^\mu/\mathrm{d}\lambda$. Using the parameterisation of Eq. (2.29) in $p^\mu = \mathrm{d}x^\mu/\mathrm{d}\lambda$, we have

$$\frac{\mathrm{d}\eta}{\mathrm{d}\lambda} = \frac{\epsilon}{a^2}(1-\psi) \tag{2.31}$$

$$\frac{\mathrm{d}x^i}{\mathrm{d}\lambda} = \frac{\epsilon}{a^2}(1+\phi)\, e^i \tag{2.32}$$

$$\Rightarrow \frac{\mathrm{d}x^i}{\mathrm{d}\eta} = (1+\phi+\psi)\, e^i, \tag{2.33}$$

at linear order.

Then the geodesic equation in conformal time (change from $\mathrm{d}\lambda$ to $\mathrm{d}\eta$) is

$$(1-\psi)\frac{\epsilon}{a^2}\frac{\mathrm{d}p^\mu}{\mathrm{d}\eta} + \Gamma^\mu_{\nu\rho} p^\nu p^\rho = 0. \tag{2.34}$$

We now want to find out what are the 0-component and i-component of this geodesic equation. We need to use the fact that the derivative $\mathrm{d}\psi/\mathrm{d}\eta$ is along the path of photon so

$$\frac{\mathrm{d}\psi}{\mathrm{d}\eta} = \dot{\psi} + e^i \partial_i \psi, \tag{2.35}$$

to the first order. In addition, we need to use the perturbed connection coefficients (Eq. (2.27)), so finally by simplifying the $\mu = 0$ component of Eq. (2.34), we have

$$\frac{1}{\epsilon}\frac{\mathrm{d}\epsilon}{\mathrm{d}\eta} = -\frac{\mathrm{d}\psi}{\mathrm{d}\eta} + (\dot{\phi} + \dot{\psi}). \tag{2.36}$$

This equation tells us how the comoving energy of a photon evolves along the photon path in the presence of metric perturbations. In the background, ϵ is a constant, but this is modified by the variation of ψ along the path (the first term on the right) and by the time evolution of gravitational potential (second term on the right). The second term is the ISW effect which is important when the dark energy starts to dominate the Universe.

By using the i-component of Eq. (2.34) and Eq. (2.29), we will find that the direction of photon propagation evolves along the photon path according to the first-order equation

$$\frac{\mathrm{d}e^i}{\mathrm{d}\eta} = -\left(\delta^{ij} - e^i e^j\right)\partial_j(\phi+\psi). \tag{2.37}$$

Just a note, in the vector format, Eq. (2.33) and Eq. (2.37) can be written as

$$\frac{\mathrm{d}\mathbf{x}}{\mathrm{d}\eta} = (1+\phi+\psi)\mathbf{e}, \quad \frac{\mathrm{d}\mathbf{e}}{\mathrm{d}\eta} = -\nabla_\perp(\phi+\psi), \tag{2.38}$$

where $\nabla_\perp = \nabla - \mathbf{e}(\mathbf{e}\cdot\nabla)$.

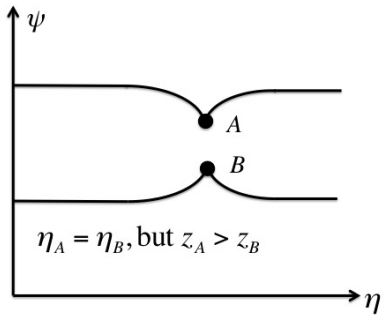

Figure 11: The diagram illustrates that, although two objects could form at the same time, and have the same evolutionary history (same η) but they could have different redshifts due to the potential effect. Therefore, the surface of constant η could have z fluctuations and the surface of constant z could have η fluctuations.

Solving for the photon path, we integrate Eq. (2.33), we have

$$\begin{aligned}
\mathbf{x}(\hat{n},\eta) &= \int_{\eta_{\rm A}}^{\eta} \frac{{\rm d}\mathbf{x}}{{\rm d}\eta}{\rm d}\eta = \int_{\eta_{\rm A}}^{\eta}(1+\phi+\psi)\mathbf{e}{\rm d}\eta \\
&= \int_{\eta_{\rm A}}^{\eta}(\phi+\psi)\mathbf{e}\,{\rm d}\eta' + \int_{\eta_{\rm A}}^{\eta}\mathbf{e}\,{\rm d}\eta' \\
&\simeq \mathbf{e}_{\rm A}\int_{\eta_{\rm A}}^{\eta}(\phi+\psi){\rm d}\eta' + (\mathbf{e}\eta')\,|_{\eta_{\rm A}}^{\eta} - \int_{\eta_{\rm A}}^{\eta}\eta'\left(\frac{{\rm d}\mathbf{e}}{{\rm d}\eta'}\right){\rm d}\eta' \\
&\simeq \mathbf{e}_{\rm A}\int_{\eta_{\rm A}}^{\eta}(\phi+\psi){\rm d}\eta' + (\mathbf{e}\eta - \mathbf{e}_{\rm A}\eta_{\rm A}) + \int_{\eta_{\rm A}}^{\eta}\eta'\vec{\nabla}_\perp(\phi+\psi){\rm d}\eta' \\
&= \mathbf{e}_{\rm A}\int_{\eta_{\rm A}}^{\eta}(\phi+\psi){\rm d}\eta' + \mathbf{e}_{\rm A}(\eta-\eta_{\rm A}) - \int_{\eta_{\rm A}}^{\eta}(\eta-\eta')\vec{\nabla}_\perp(\phi+\psi){\rm d}\eta', \qquad (2.39)
\end{aligned}$$

where the second term indicates the radial displacement and corresponds to (Shapiro) time-delay, and the third term is the transverse (lensing) displacement. The reason that in the first term we approximate $\mathbf{e} = \mathbf{e}_{\rm A}$ is the *Born Approximation* in the sense that for small perturbation, the lensing integral can be evaluated on the unperturbed light path. At first-order this is fine because the $\mathbf{e}$ is multiplied with $(\phi+\psi)$, so it is fine to assume $\mathbf{e}$ takes its zeroth-order value, i.e. a constant $\mathbf{e}_{\rm A}$.

Born Approximation: In Quantum Mechanics, if the potential $V(r)$ is weak enough, it will distort only slightly the incident plane wave. Therefore one can replace the scattered wave function $\Psi(r)$ by a plane wave.

2.2.4 Brightness temperature fluctuation

Now we can calculate the brightness temperature fluctuation as a function of redshift z and direction $\hat{\mathbf{n}}$ on the sky. According to Eq. (2.11), we need to expand $n_{\rm HI}$ and $|{\rm d}\lambda/{\rm d}z|$ since other

terms are constants.

$n_{\rm HI}$ term. First of all, we have to make clear that z is observed redshift and η is the conformal time. The perturbed conformal time at redshift z along the line-of-sight $\hat{\mathbf{n}}$ is $\eta(\hat{\mathbf{n}}, z) = \overline{\eta}_z + \delta\eta$, where $\overline{\eta}_z$ is the unperturbed value (see Fig. 11). So $\delta\eta$ is the time variation at a given z at a particular direction. This is similar to the CMB where if you look at different parts of the sky you see different temperature, although local temperature at the decoupling time is the same.

We now calculate the perturbation of neutral hydrogen density at redshift z at a given direction

$$n_{\rm HI}\left(z, \hat{\mathbf{n}}\right) = \overline{n}_{\rm HI}\left(\overline{\eta}_z\right)\left(1 + \delta_n + \frac{\dot{\overline{n}}_{\rm HI}}{\overline{n}_{\rm HI}}\delta\eta\right), \tag{2.40}$$

where the second term is the intrinsic brightness fluctuation, and the third term is due to the perturbation of conformal time.

Preparation for calculating $|{\rm d}\lambda/{\rm d}z|$ term. Let us write the source 4-velocity as $u^a_{\rm s} = u^a + v^a$, i.e.$u^\mu_{\rm s} = a^{-1}[1-\psi, v^i]$, where v^i is the orthonormal-triad component of v^a. Similarly, observer's 4-velocity at point A can be written as $u^\mu_{\rm oA} = a_{\rm A}^{-1}[1-\phi_{\rm A}, v^i_{\rm oA}]$. Therefore, the physical energy of the photon at emission time E and at receiving time $E_{\rm A}$ ($E_{\rm A}$ is the energy of a fundamental observer with rest to the FRW frame) is related to the observed redshift through

$$(1+z) = \left(\frac{E}{E_{\rm A}}\right)(1 + \hat{\mathbf{n}}\cdot(\mathbf{v} - \mathbf{v}_{\rm oA})), \tag{2.41}$$

where z is the observed redshift which contains both physical redshift factor and the local motion contribution. One can see that if a photon is moving away from the observer, $\hat{\mathbf{n}}\cdot\mathbf{v} > 0$, then it make z increase (redshift) and vice versa. For local motion, if observer moves towards the observing line-of-sight direction, i.e. $\hat{\mathbf{n}}\cdot\mathbf{v}_{\rm oA} > 0$, it makes the line-of-sight direction z decrease (blueshift). $\hat{\mathbf{n}} = -\mathbf{e}_{\rm A}$ is the line-of-sight direction of the photon seen by the observer. Using the definition of comoving energy, we have

$$1 + z = \left(\frac{a_{\rm A}}{a}\frac{\epsilon}{\epsilon_{\rm A}}\right)(1 + \hat{\mathbf{n}}\cdot(\mathbf{v} - \mathbf{v}_{\rm oA}))\,. \tag{2.42}$$

Integrating Eq. (2.36), we obtain the ratio of Newtonian gauge energies

$$\frac{\epsilon}{\epsilon_{\rm A}} = 1 + \psi_{\rm A} - \psi + \int_{\eta_{\rm A}}^{\eta}(\dot{\phi} + \dot{\psi}){\rm d}\eta', \tag{2.43}$$

which has the usual Sachs-Wolfe (first term) and integrated Sachs-Wolfe (ISW) (second term) contributions. Substituting Eq. (2.43) into Eq. (2.42), we have the redshift at η along the line-of-sight $\hat{\mathbf{n}}$ as

$$1 + z = \frac{a_{\rm A}}{a(\eta)}\left(1 + \psi_{\rm A} - \psi + \int_{\eta_{\rm A}}^{\eta}(\dot{\phi} + \dot{\psi}){\rm d}\eta' + \hat{\mathbf{n}}\cdot(\mathbf{v} - \mathbf{v}_{\rm oA})\right), \tag{2.44}$$

note that this z is the redshift at η. Again, we use $\eta(\hat{\mathbf{n}}, z) = \overline{\eta}_z + \delta\eta$, where $\overline{\eta}_z$ is the unperturbed value (see Fig. 11). Therefore, we have

$$1 + z = \frac{a_{\rm A}}{a(\overline{\eta}_z)} = \frac{a_{\rm A}}{a(\eta)} \left(1 + \psi_{\rm A} - \psi + \int_{\eta_{\rm A}}^{\eta} (\dot{\phi} + \dot{\psi}) {\rm d}\eta' + \hat{\mathbf{n}} \cdot (\mathbf{v} - \mathbf{v}_{\rm oA})\right) \tag{2.45}$$

$$\Rightarrow \quad \frac{a(\eta)}{a(\overline{\eta}_z)} = 1 + \psi_{\rm A} - \psi + \int_{\eta_{\rm A}}^{\eta} (\dot{\phi} + \dot{\psi}) {\rm d}\eta' + \hat{\mathbf{n}} \cdot (\mathbf{v} - \mathbf{v}_{\rm oA}), \tag{2.46}$$

since $a(\eta) = a(\overline{\eta}_z)(1 + \mathcal{H}\delta\eta)$, one can obtain

$$\mathcal{H}(\overline{\eta}_z)\delta\eta = \psi_{\rm A} - \psi + \int_{\eta_{\rm A}}^{\overline{\eta}_z} (\dot{\phi} + \dot{\psi}) {\rm d}\eta' + \hat{\mathbf{n}} \cdot (\mathbf{v} - \mathbf{v}_{\rm oA}), \tag{2.47}$$

where we have substituted $\eta \to \overline{\eta}_z$ into the above equation since the difference is second order. $\mathcal{H} \equiv \dot{a}/a$ is the conformal Hubble parameter. Note that in Eq. (2.47) the ISW term ϕ and ψ are functions of spatial hyper-surface $\mathbf{r}$ at each conformal time η', so $\delta\eta$ is both a function of $\hat{\mathbf{n}}$ on the sky and a function of redshift z.

$|{\rm d}\lambda/{\rm d}z|$ term. Now we can calculate $|{\rm d}\lambda/{\rm d}z|$. We first calculate $|{\rm d}\lambda/{\rm d}z|(\eta)$ and then expand $\eta(\hat{\mathbf{n}}, z) = \overline{\eta}_z + \delta\eta$. First, we have

$$\left|\frac{{\rm d}\lambda}{{\rm d}z}\right|_\eta = \left|\left(\frac{{\rm d}\lambda}{{\rm d}\eta}\right)\left(\frac{{\rm d}\eta}{{\rm d}z}\right)\right|. \tag{2.48}$$

From Eq. (2.31), we have

$$\begin{aligned}
\frac{{\rm d}\eta}{{\rm d}\lambda} &= \frac{\epsilon}{a^2}(1 - \psi) = \frac{1}{aa_{\rm A}}\left(\frac{a_{\rm A}}{a}\right)\left(\left(\frac{\epsilon}{\epsilon_{\rm A}}\right)\epsilon_{\rm A}\right)(1 - \psi) = \left(\frac{\epsilon_{\rm A}}{aa_{\rm A}}\right)\left(\frac{\epsilon}{\epsilon_{\rm A}}\frac{a_{\rm A}}{a}\right)(1 - \psi) \\
&= \left(\frac{\epsilon_{\rm A}}{aa_{\rm A}}\right)(1 + z)\left(1 - \psi - \hat{\mathbf{n}} \cdot (\mathbf{v} - \mathbf{v}_{\rm oA})\right), \qquad (2.49) \\
\Rightarrow \frac{{\rm d}\lambda}{{\rm d}\eta} &= \left(\frac{aa_{\rm A}}{\epsilon_{\rm A}(1 + z)}\right)(1 + \psi + \hat{\mathbf{n}} \cdot (\mathbf{v} - \mathbf{v}_{\rm oA})) \qquad (2.50)
\end{aligned}$$

where in the second line of Eq. (2.49) we have used the Eq. (2.42). Then by using Eq. (2.45) we have

$$\begin{aligned}
\frac{{\rm d}z}{{\rm d}\eta} &= \frac{a_{\rm A}}{a(\eta)}\left[-\frac{{\rm d}\psi}{{\rm d}\eta} + (\dot{\phi} + \dot{\psi}) + \hat{\mathbf{n}} \cdot \frac{{\rm d}\mathbf{v}}{{\rm d}\eta}\right] - \frac{a_{\rm A}}{a^2}\frac{{\rm d}a}{{\rm d}\eta}\left[1 + \psi_{\rm A} - \psi + \int_{\eta_{\rm A}}^{\eta} (\dot{\phi} + \dot{\psi}) {\rm d}\eta' + \hat{\mathbf{n}} \cdot (\mathbf{v} - \mathbf{v}_{\rm oA})\right] \\
&= -\frac{\mathcal{H}(\eta)a_{\rm A}}{a(\eta)}\left(1 + \psi_{\rm A} - \psi + \int_{\eta_{\rm A}}^{\eta} (\dot{\phi} + \dot{\psi}) {\rm d}\eta' + \hat{\mathbf{n}} \cdot (\mathbf{v} - \mathbf{v}_{\rm oA}) + \frac{1}{\mathcal{H}}\frac{{\rm d}\psi}{{\rm d}\eta} - \frac{1}{\mathcal{H}}(\dot{\phi} + \dot{\psi}) - \frac{1}{\mathcal{H}}\hat{\mathbf{n}} \cdot \frac{{\rm d}\mathbf{v}}{{\rm d}\eta}\right).
\end{aligned} \tag{2.51}$$

We invert Eq. (2.51) and multiply with Eq. (2.50), we obtain

$$\begin{aligned}
\left.\frac{{\rm d}\lambda}{{\rm d}z}\right|_\eta &= -\frac{a^2(\eta)}{\mathcal{H}(\eta)\epsilon_{\rm A}(1 + z)}\left[1 - \psi_{\rm A} + 2\psi - \int_{\eta_{\rm A}}^{\eta} (\dot{\phi} + \dot{\psi}) {\rm d}\eta' - \frac{1}{\mathcal{H}}\frac{{\rm d}\psi}{{\rm d}\eta} + \frac{1}{\mathcal{H}}(\dot{\phi} + \dot{\psi}) + \frac{1}{\mathcal{H}}\hat{\mathbf{n}} \cdot \frac{{\rm d}\mathbf{v}}{{\rm d}\eta}\right] \\
&= -\frac{a^2(\eta)}{\mathcal{H}(\eta)\epsilon_{\rm A}(1 + z)}\left[1 + \psi - \mathcal{H}(\overline{\eta}_z)\delta\eta + \hat{\mathbf{n}} \cdot (\mathbf{v} - \mathbf{v}_{\rm oA}) - \frac{1}{\mathcal{H}}\frac{{\rm d}\psi}{{\rm d}\eta} + \frac{1}{\mathcal{H}}(\dot{\phi} + \dot{\psi}) + \frac{1}{\mathcal{H}}\hat{\mathbf{n}} \cdot \frac{{\rm d}\mathbf{v}}{{\rm d}\eta}\right],
\end{aligned} \tag{2.52}$$

where in the second line we have used Eq. (2.47) to get rid of the integral term. Now we need to calculate $|\mathrm{d}\lambda/\mathrm{d}z|$ at a given redshift z, therefore we need to expand the front term in Eq. (2.52)

$$\begin{aligned}\frac{a^2(\eta)}{\mathcal{H}(\eta)\epsilon_{\rm A}(1+z)} &= \frac{a(\overline{\eta}_z)^2\left(1+2(\dot{a}(\overline{\eta}_z)/a(\overline{\eta}_z))\delta\eta\right)}{\mathcal{H}(\overline{\eta}_z)\left(1+(\dot{\mathcal{H}}/\mathcal{H})\delta\eta\right)\epsilon_{\rm A}(1+z)} \\ &= \frac{a(\overline{\eta}_z)^2}{\mathcal{H}(\overline{\eta}_z)\epsilon_{\rm A}(1+z)}\left(1+\left(2\mathcal{H}-\frac{\dot{\mathcal{H}}}{\mathcal{H}}\right)\delta\eta\right). \end{aligned} \tag{2.53}$$

$(\epsilon_{\rm A}/a(\overline{\eta}_z))$ term. We now need to calculate $(\epsilon_{\rm A}/a(\overline{\eta}_z))$ to proceed. This is non-trivial and easy to be incorrect, and one has to bear in mind that $\epsilon_{\rm A}$ is the comoving energy of the *fundamental* observer A at rest in the Newtonian gauge, so we can call it "Newtonian gauge observer". In fact, all ϵs are comoving energy measured by Newtonian gauge observer, so that is why in Eq. (2.43), when we compare the two comoving energies, there is no Doppler term in it. But in reality neither observers or emitters are at rest in the Newtonian gauge because of the peculiar motion. Therefore $\epsilon/a = E_{21}(1-\hat{\mathbf{n}}\cdot\mathbf{v})$ because the 21-cm emitter (gas) has motion $\mathbf{v}$. Now we have two ways to calculate it

- We can write

$$\begin{aligned}\left(\frac{\epsilon_{\rm A}}{a(\overline{\eta}_z)}\right) &= \left(\frac{\epsilon_{\rm A}}{\epsilon}\right)\left(\frac{\epsilon}{a}\right)\left(\frac{a}{a(\overline{\eta}_z)}\right) \\ &= [1-f(\eta)]\left[E_{21}(1-\hat{\mathbf{n}}\cdot\mathbf{v})\right][1+f(\eta)+\hat{\mathbf{n}}\cdot(\mathbf{v}-\mathbf{v}_{\rm oA})] \\ &= E_{21}(1-\hat{\mathbf{n}}\cdot\mathbf{v}_{\rm oA}). \end{aligned} \tag{2.54}$$

  On the second line of above equation, $f(\eta) = \psi_{\rm A} - \psi + \int_{\eta_{\rm A}}^{\eta}(\dot{\phi}+\dot{\psi})\mathrm{d}\eta'$. $(\epsilon_{\rm A}/\epsilon)$ is the ratio between the comoving energy of *fundamental* receiver and emitter so we used Eq. (2.43). For $a/a(\overline{\eta}_z)$ we used Eq. (2.46).

- We can also write

$$\left(\frac{\epsilon_{\rm A}}{a(\overline{\eta}_z)}\right) = \left(\frac{\epsilon_{\rm A}}{a_{\rm A}}\right)\left(\frac{a_{\rm A}}{a(\overline{\eta}_z)}\right). \tag{2.55}$$

  $\epsilon_{\rm A}/a_{\rm A} = E_{\rm A}$, which is the energy received by fundamental observer, and $E_{\rm A}/E_{21} = (1-\hat{\mathbf{n}}\cdot\mathbf{v})/(1+\overline{z})$, where $\overline{z}$ is the redshift of only-cosmic expansion effect (no peculiar motion effect), and $\mathbf{v}$ is the peculiar velocity of emitter. This is because $\epsilon_{\rm A}/a_{\rm A}$ is the photon energy measured by a Newtonian gauge observer, whereas E_{21} is the energy measured by emitter, whose velocity differs from that of Newtonian gauge observers by the peculiar velocity of the gas v.

  In addition,

$$\frac{a_{\rm A}}{a(\overline{\eta}_z)} = (1+z) = (1+\overline{z})(1+\mathbf{n}\cdot(\mathbf{v}-\mathbf{v}_{\rm oA})), \tag{2.56}$$

  where the first equality comes from Eq. (2.45), and the second equality is just a summation effect of pure cosmic expansion and peculiar motion. Therefore, by combining the above

equations, one can find

$$\left(\frac{\epsilon_{\rm A}}{a(\overline{\eta}_z)}\right) = \left(\frac{\epsilon_{\rm A}}{a_{\rm A}}\right)\left(\frac{a_{\rm A}}{a(\overline{\eta}_z)}\right) = E_{21}\times\frac{1-\hat{\mathbf{n}}\cdot\mathbf{v}}{1+\overline{z}}(1+\overline{z})(1+\mathbf{n}\cdot(\mathbf{v}-\mathbf{v}_{\rm oA})) = E_{21}(1-\hat{\mathbf{n}}\cdot\mathbf{v}_{\rm oA}), \quad (2.57)$$

which is the same conclusion as Eq. (2.54). Note that This cancels the Doppler term of observer's motion in Eq. (2.52).

Putting together for $T_{\rm b}(z,\hat{\mathbf{n}})$. Therefore, combining Eqs. (2.53) with (2.52) and ((2.54) or (2.57)), we have

$$\left|\frac{{\rm d}\lambda}{{\rm d}z}\right|(z,\hat{\mathbf{n}}) = \frac{a(\overline{\eta}_z)}{\mathcal{H}(\overline{\eta}_z)E_{21}(1+z)}\left[1-\left(\frac{\dot{\mathcal{H}}}{\mathcal{H}}-\mathcal{H}\right)\delta\eta+\psi+\hat{\mathbf{n}}\cdot\mathbf{v}-\frac{1}{\mathcal{H}}\frac{{\rm d}\psi}{{\rm d}\eta}+\frac{1}{\mathcal{H}}(\dot{\phi}+\dot{\psi})+\frac{1}{\mathcal{H}}\hat{\mathbf{n}}\cdot\frac{{\rm d}\mathbf{v}}{{\rm d}\eta}\right]. \quad (2.58)$$

Combining Eq. (2.11) with Eq. (2.40) and Eq. (2.58), we obtain

$$\begin{aligned} T_{\rm b}(z,\hat{\mathbf{n}}) &= \left(\frac{3}{32\pi}\right)\frac{(h_{\rm p}c)^3\overline{n}_{\rm HI}(\overline{\eta}_z)A_{10}}{k_{\rm B}E_{21}^2(1+z)H(z)}\left(1+\Delta_{T_{\rm b}}(z,\hat{\mathbf{n}})\right) \\ \Delta_{T_{\rm b}}(z,\hat{\mathbf{n}}) &= \delta_n+\frac{\dot{\overline{n}}_{\rm HI}}{\overline{n}_{\rm HI}}\delta\eta-\left(\frac{\dot{\mathcal{H}}}{\mathcal{H}}-\mathcal{H}\right)\delta\eta+\psi+\hat{\mathbf{n}}\cdot\mathbf{v}-\frac{1}{\mathcal{H}}\frac{{\rm d}\psi}{{\rm d}\eta}+\frac{1}{\mathcal{H}}(\dot{\phi}+\dot{\psi})+\frac{1}{\mathcal{H}}\hat{\mathbf{n}}\cdot\frac{{\rm d}\mathbf{v}}{{\rm d}\eta}. \end{aligned} \quad (2.59)$$

Here we use a few facts to simplify the above equation. The first thing is that if the comoving number density of HI is conserved at low redshift (i.e. ionized fraction of hydrogen is constant), then $\overline{n}_{\rm HI}\sim a^{-3}$, then $(\overline{n}_{\rm HI}a^3)$ is a constant. But we are not sure whether this is true, so in general case the following equation represents the change of ionized fraction of HI

$$\frac{{\rm d}\ln(a^3\overline{n}_{\rm HI})}{{\rm d}\eta} = \frac{1}{(a^3\overline{n}_{\rm HI})}\frac{{\rm d}(a^3\overline{n}_{\rm HI})}{{\rm d}\eta} = 3\mathcal{H}+\frac{\dot{\overline{n}}_{\rm HI}}{\overline{n}_{\rm HI}}. \quad (2.60)$$

The second equation is the directional derivative of η can be broken down into two terms

$$\begin{aligned} \frac{{\rm d}\mathbf{v}}{{\rm d}\eta} &= \left.\frac{\partial\mathbf{v}}{\partial\eta}\right|_{\mathbf{x}}-(\hat{\mathbf{n}}\cdot\vec{\nabla})\mathbf{v} \\ \frac{{\rm d}\psi}{{\rm d}\eta} &= \left.\frac{\partial\psi}{\partial\eta}\right|_{\mathbf{x}}-(\hat{\mathbf{n}}\cdot\vec{\nabla})\psi, \end{aligned} \quad (2.61)$$

where the first term is partial derivative, and second term is the spatial derivative. The reason that the second term is negative sign is because η increases if the direction is towards the observer, while $\hat{\mathbf{n}}$ is the line-of-sight direction leaving from observer to the sky, so the two directions are opposite.

The third equation we will use is the Euler equation $\dot{\mathbf{v}}+\mathcal{H}\mathbf{v}+\nabla\psi=0$, where $\dot{\mathbf{v}}=\partial\mathbf{v}/\partial\eta$. Therefore, by substituting these three relations into Eq. (2.59), we can simply it as

$$\Delta_{T_{\rm b}}(z,\hat{\mathbf{n}}) = \delta_n-\frac{1}{\mathcal{H}}\left[\hat{\mathbf{n}}\cdot(\hat{\mathbf{n}}\cdot\vec{\nabla})\mathbf{v}\right]+\left(\frac{{\rm d}\ln(a^3\overline{n}_{\rm HI})}{{\rm d}\eta}-\frac{\dot{\mathcal{H}}}{\mathcal{H}}-2\mathcal{H}\right)\delta\eta+\frac{1}{\mathcal{H}}\dot{\phi}+\psi \quad (2.62)$$

The second term means

$$\hat{\mathbf{n}} \cdot (\hat{\mathbf{n}} \cdot \vec{\nabla})\mathbf{v} = \sum_{i,j} \hat{\mathbf{n}}_i (\hat{\mathbf{n}}_j \cdot \nabla_j) v_i. \tag{2.63}$$

Each of the term in Eq. (2.62) has special meaning. The first two terms are the usual density and redshift-space distortion term, the third term comes from the evaluating the zero-order brightness temperature at the perturbed time corresponding to the observed redshift. The fourth term is the ISW term. The fifth term (ψ) is due to the conversion between radial distance in gas frame ($\mathrm{d}\lambda$) with increments in redshift ($\mathrm{d}z$), i.e. comes from $|\mathrm{d}\lambda/\mathrm{d}z|$ term.

2.2.5 Doppler shift

The Eq. (2.62) gives the HI gas fluctuation as seen by any observer in their own rest frame. The dependence of observer's own motion is through Eq. (2.47) into the $\delta\eta$ term in Eq. (2.62). This is equivalent to the frame transformation via

$$(1+z')T'_{\rm b}(z', \hat{\mathbf{n}}') = (1+z)T_{\rm b}(z, \hat{\mathbf{n}}), \tag{2.64}$$

which follows the invariant distribution function. Since $(1+z) = (1+z')(1+\hat{\mathbf{n}} \cdot \mathbf{v}_{\rm rel})$, where $\mathbf{v}_{\rm rel}$ is the relative velocity of frame with redshift z' to the frame with redshift z. From this equation, we obtain $(z-z') = (1+z')(1+\hat{\mathbf{n}} \cdot \mathbf{v}_{\rm rel})$. Now we can calculate the relation between perturbation in two frames.First

$$T'_{\rm b}(z', \hat{\mathbf{n}}') = \left(\frac{1+z}{1+z'}\right) T_{\rm b}(z, \hat{\mathbf{n}}) = (1 + \hat{\mathbf{n}} \cdot \mathbf{v}_{\rm rel}) T_{\rm b}(z, \hat{\mathbf{n}}). \tag{2.65}$$

We then expand the l.h.s and r.h.s separately

$$T'_{\rm b}(z', \hat{\mathbf{n}}') \simeq \overline{T}_{\rm b}(z')(1 + \Delta'_{T_{\rm b}}(z', \hat{\mathbf{n}}')), \tag{2.66}$$

$$\begin{aligned} T_{\rm b}(z, \hat{\mathbf{n}}) &\simeq T_{\rm b}(z', \hat{\mathbf{n}}) + \left(\frac{\mathrm{d}T_{\rm b}(z)}{\mathrm{d}z}\right)_{z'} \cdot (z - z') \\ &\simeq \overline{T}_{\rm b}(z')(1 + \Delta_{T_{\rm b}}(z', \hat{\mathbf{n}})) + \left(\frac{\mathrm{d}\overline{T}_{\rm b}(z)}{\mathrm{d}z}\right)_{z'} \cdot (z - z') \\ &= \overline{T}_{\rm b}(z') \left[1 + \Delta_{T_{\rm b}}(z', \hat{\mathbf{n}}) + \frac{\mathrm{d}\ln \overline{T}_{\rm b}(z')}{\mathrm{d}z'}(1+z')(1 + \hat{\mathbf{n}} \cdot \mathbf{v}_{\rm rel})\right]. \end{aligned} \tag{2.67}$$

Combining Eqs. (2.65), (2.66) and (2.67), we have

$$\Delta'_{T_{\rm b}}(z', \hat{\mathbf{n}}') = \Delta_{T_{\rm b}}(z', \hat{\mathbf{n}}) + \hat{\mathbf{n}} \cdot \mathbf{v}_{\rm rel} + \frac{\mathrm{d}\ln \overline{T}_{\rm b}(z')}{\mathrm{d}z'}(1+z')(1 + \hat{\mathbf{n}} \cdot \mathbf{v}_{\rm rel}). \tag{2.68}$$

All of the $\hat{\mathbf{n}} \cdot \mathbf{v}_{\rm rel}$ terms only affect the $\ell = 1$ moment.

2.2.6 Why lensing isn't important at first order?

Comparing the perturbation of surface brightness temperature (Eq. (2.62)) with the perturbation of the source number counts (eq. (28) in [9]), one will find that the source number counts contain

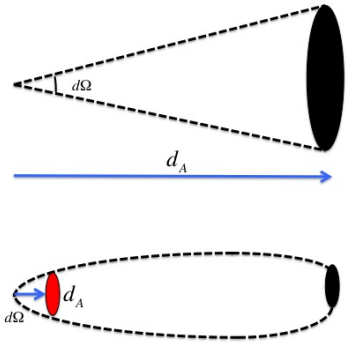

Figure 12: The measured surface brightness at a given solid angle (i.e. amount of energy per solid angle) is determined by the product of the number of sources in the solid angle and the flux of the source. This figure shows that, while lensing is turned on, although the total number of sources per solid angle decreases, lensing magnification increases the flux of each source. This is equivalent to the decrease of angular diameter distance. Therefore, the surface brightness one measures stay the same.

the perturbed equation of Jacobi map, which contains lensing. However, for surface brightness, it does not contain lensing contribution. To see lensing has no contribution to the surface brightness variation, one use Fig. 12 to understand this point. Suppose you observe a patch of the sky for a given solid angle with volume $\mathrm{d}V = (\det D_\mathrm{o})\mathrm{d}\Omega\mathrm{d}l \sim \mathrm{d}N_\mathrm{source}$. The flux of the source is $\mathrm{d}F \sim L/\det D_\mathrm{o}$. Therefore $\mathrm{d}T_\mathrm{b} \sim \mathrm{d}F\mathrm{d}N_\mathrm{source} \sim L\mathrm{d}\Omega\mathrm{d}l$. The meaning is this: If you turn on lensing, the number of sources that you measure ($\mathrm{d}N_\mathrm{source}$) is going down, but the flux of the source is going up due to the lensing magnification effect (just like you place the source at smaller angular diameter distance but with same $\mathrm{d}\Omega$, shown in Fig. 12). Therefore the surface brightness you measure is not changed.

One can see this more quantitatively through the perturbation of luminosity distance. In Eq. (2.11), the n_HI is the physical density of HI in the source, which is related to the observed HI atom density per solid angle and per redshift $n_\mathrm{HI}^\mathrm{obs}(z,\hat{\mathbf{n}})$ through $n_\mathrm{HI}^\mathrm{obs}(z,\hat{\mathbf{n}})\mathrm{d}z\mathrm{d}\Omega = n_\mathrm{HI}\,\mathrm{d}V$, where $\mathrm{d}V = \mathrm{d}\tilde{A}(u_\mathrm{s}^a k_a)\mathrm{d}\lambda$. Therefore, one can transform Eq. (2.11) into

$$T_\mathrm{b}(z,\hat{\mathbf{n}}) = \frac{3h_\mathrm{p}^3 A_{10}}{32\pi k_\mathrm{B} E_{21}}\left(\frac{n_\mathrm{HI}^\mathrm{obs}(z,\hat{\mathbf{n}})\mathrm{d}z\mathrm{d}\Omega}{\mathrm{d}\tilde{A}(u_\mathrm{s}^a k_a)\mathrm{d}\lambda}\right)\left|\frac{\mathrm{d}\lambda}{\mathrm{d}z}\right|, \tag{2.69}$$

and note that $u_\mathrm{s}^a k_a = E_{21}$ and $\mathrm{d}\tilde{A}/\mathrm{d}\Omega = \det\mathcal{D}_\mathrm{o}$, where $\mathcal{D}_\mathrm{o}$ is the determinant of the Jacobi map in the observer's frame [10]. Therefore, Eq. (2.69) can be simplified as

$$T_\mathrm{b}(z,\hat{\mathbf{n}}) = \frac{3h_\mathrm{p}^3 A_{10}}{32\pi k_\mathrm{B} E_{21}^2}\frac{n_\mathrm{HI}^\mathrm{obs}(z,\hat{\mathbf{n}})}{\det\mathcal{D}_\mathrm{o}}, \tag{2.70}$$

which is exactly the sense we show in Fig. 12, i.e. surface brightness is equal to the product of observed number density times the flux of each source.

To further see the cancellation of luminosity diameter distance perturbation, which include lensing, we notice that $d_{\rm L}^2 = (1+z)^4 {\rm det}D_{\rm o}$, therefore

$$\Delta_{T_{\rm b}}(z,\hat{\mathbf{n}}) = \Delta_n(z,\hat{\mathbf{n}}) - \frac{\delta({\rm det}D_{\rm o})}{{\rm det}D_{\rm o}} = \Delta_n(z,\hat{\mathbf{n}}) - 2\frac{\delta d_{\rm L}(z,\hat{\mathbf{n}})}{\bar{d}_{\rm L}(z)}. \tag{2.71}$$

The perturbation of the determinant of the Jacobian map at observer's rest frame is given by eq. (20) in [9], where the 5 terms after 1 are the perturbations. The last term is the abberation effect. One can see that, by subtracting this term from the number count perturbation (eq. (28) in [9]), we will end up in surface brightness fluctuation (Eq. (2.62) here).

2.2.7 From theory to observables

We now want to transform the real-space density contrast (Eq. (2.62)) into the k-space, and figure out the angular power spectrum in ℓ-space.

In general, we have

$$\begin{aligned}
\Delta_{T_{\rm b}}(z,\hat{\mathbf{n}}) &= \int \frac{{\rm d}^3\mathbf{k}}{(2\pi)^{3/2}} \Delta_{T_{\rm b}}(z,\mathbf{k},\hat{\mathbf{n}}) {\rm e}^{i\mathbf{k}\cdot\mathbf{r}(\hat{\mathbf{n}},z)} \\
&= \int \frac{{\rm d}^3\mathbf{k}}{(2\pi)^{3/2}} \Delta_{T_{\rm b}}(z,\mathbf{k},\hat{\mathbf{n}}) \left[4\pi \sum_{\ell m} i^\ell j_\ell(k\chi) Y^*_{\ell m}(\hat{\mathbf{k}}) Y_{\ell m}(\hat{\mathbf{n}}) \right], \\
&= \sum_{\ell m} \left[\int \frac{{\rm d}^3\mathbf{k}}{(2\pi)^{3/2}} \Delta_{T_{\rm b}}(z,\mathbf{k},\hat{\mathbf{n}}) (4\pi i^\ell) j_\ell(k\chi) Y^*_{\ell m}(\hat{\mathbf{k}}) \right] Y_{\ell m}(\hat{\mathbf{n}}) \\
&\equiv \sum_{\ell m} \left[(4\pi i^\ell) \int \frac{{\rm d}^3\mathbf{k}}{(2\pi)^{3/2}} \Delta_{T_{\rm b},\ell}(z,\mathbf{k}) Y^*_{\ell m}(\hat{\mathbf{k}}) \right] Y_{\ell m}(\hat{\mathbf{n}}).
\end{aligned} \tag{2.72}$$

The last line is our definition, and we want to move all of the dependence of $\hat{\mathbf{n}}$ into $Y_{\ell m}(\hat{\mathbf{n}})$ so that $\Delta_{T_{\rm b},\ell}(z,\mathbf{k})$ is really the Fourier space density contrast of ℓ-mode.

We now start to figure out how each term in Eq. (2.62) is transformed. For the first, fourth and fifth term in Eq. (2.62), it is the density contrast, ISW and potential term in the real-space, therefore its Fourier transform is

$$\Delta^{(1,4,5)}_{T_{\rm b}}(z,\hat{\mathbf{n}}) = \int \frac{{\rm d}^3\mathbf{k}}{(2\pi)^{3/2}} \mathcal{F}\left[\delta_n + \frac{1}{\mathcal{H}}\dot{\phi} + \psi \right] {\rm e}^{i\mathbf{k}\cdot\mathbf{r}}, \tag{2.73}$$

where $\mathcal{F}$ just represents the Fourier transformation. In the following, we will use a "$\sim$" to represent the Fourier function.

In addition, we will frequently use the following plane-wave expansion

$${\rm e}^{i\mathbf{k}\cdot\mathbf{r}(\hat{\mathbf{n}},z)} = \sum_{\ell m} (4\pi i^\ell) j_\ell(k\chi) Y^*_{\ell m}(\hat{\mathbf{k}}) Y_{\ell m}(\hat{\mathbf{n}}), \tag{2.74}$$

where $\chi(z)$ is the comoving distance to redshift z.

By using Eq. (2.74), Eq. (2.73) becomes

$$\begin{aligned}
\Delta^{(1,4,5)}_{T_{\rm b}}(z,\hat{\mathbf{n}}) &= \int \frac{{\rm d}^3\mathbf{k}}{(2\pi)^{3/2}}\left[\tilde{\delta}_n + \frac{1}{\mathcal{H}}\dot{\tilde{\phi}} + \tilde{\psi}\right]\left[\sum_{\ell m}(4\pi i^\ell) j_\ell(k\chi) Y^*_{\ell m}(\hat{\mathbf{k}}) Y_{\ell m}(\hat{\mathbf{n}})\right] \\
&= \sum_{\ell m} Y_{\ell m}(\hat{\mathbf{n}})\left[(4\pi i^\ell)\int \frac{{\rm d}^3\mathbf{k}}{(2\pi)^{3/2}}\left(\tilde{\delta}_n + \frac{1}{\mathcal{H}}\dot{\tilde{\phi}} + \tilde{\psi}\right) j_\ell(k\chi) Y^*_{\ell m}(\hat{\mathbf{k}})\right] \\
\Rightarrow \Delta^{(1,4,5)}_{T_{\rm b},\ell}(z,\mathbf{k}) &= \left(\tilde{\delta}_n + \frac{1}{\mathcal{H}}\dot{\tilde{\phi}} + \tilde{\psi}\right) j_\ell(k\chi), \qquad (2.75)
\end{aligned}$$

where the last line is by comparing Eq. (2.75) with Eq. (2.72).

For the second term, i.e. Redshift-Space-Distortion term (RSD), we first define the velocity field in real and Fourier space

$$\mathbf{v}(\mathbf{r}) = \int \frac{{\rm d}^3\mathbf{k}}{(2\pi)^{3/2}}\tilde{\mathbf{v}}(\mathbf{k}){\rm e}^{i\mathbf{k}\cdot\mathbf{r}}. \qquad (2.76)$$

Here note the dimension. $\mathbf{v}(\mathbf{r})$ has the dimension $[{\rm LT}^{-1}]$, so $\tilde{\mathbf{v}}(\mathbf{k})$ has the dimension $[{\rm L}^3{\rm T}^{-1}]$. In order to preserve the dimension, we define the scalar $\tilde{v}(\mathbf{k})$ as [8]

$$\mathbf{v}(\mathbf{k}) = -i\hat{\mathbf{k}}\tilde{v}(\mathbf{k}), \qquad (2.77)$$

so that it has the same dimension as $\mathbf{v}(\mathbf{k})$. Therefore, the Fourier transformation of the RSD term is

$$\mathcal{F}\left[-\frac{1}{\mathcal{H}}\hat{\mathbf{n}}\cdot(\hat{\mathbf{n}}\cdot\vec{\nabla}\mathbf{v})\right] = -\frac{1}{\mathcal{H}}(\hat{\mathbf{k}}\cdot\hat{\mathbf{n}})^2 k\tilde{v}(\mathbf{k}) \qquad (2.78)$$

Therefore,

$$\begin{aligned}
\Delta^{(2)}_{T_{\rm b}}(z,\hat{\mathbf{n}}) &= \int \frac{{\rm d}^3\mathbf{k}}{(2\pi)^{3/2}}\mathcal{F}\left[-\frac{1}{\mathcal{H}}\hat{\mathbf{n}}\cdot(\hat{\mathbf{n}}\cdot\vec{\nabla}\mathbf{v})\right]{\rm e}^{i\mathbf{k}\cdot\mathbf{r}} \\
&= -\frac{1}{\mathcal{H}}\int \frac{{\rm d}^3\mathbf{k}}{(2\pi)^{3/2}}(\tilde{v}(\mathbf{k})(\hat{\mathbf{k}}\cdot\hat{\mathbf{n}})^2 k){\rm e}^{i\mathbf{k}\cdot\mathbf{r}}. \qquad (2.79)
\end{aligned}$$

Since

$$\frac{\partial}{\partial\chi}{\rm e}^{i\mathbf{k}\cdot\mathbf{r}} = \frac{\partial}{\partial\chi}{\rm e}^{i(\mathbf{k}\cdot\hat{\mathbf{n}})\chi} = (i\hat{n}^i k_i){\rm e}^{i\mathbf{k}\cdot\mathbf{r}} \Rightarrow \frac{\partial^2}{\partial\chi^2}{\rm e}^{i\mathbf{k}\cdot\mathbf{r}} = -(\hat{n}^i k_i)(\hat{n}^j k_j){\rm e}^{i\mathbf{k}\cdot\mathbf{r}} = -(\mathbf{k}\cdot\hat{\mathbf{n}})^2{\rm e}^{i\mathbf{k}\cdot\mathbf{r}}, \qquad (2.80)$$

then Eq. (2.79) becomes

$$\begin{aligned}
\Delta^{(2)}_{T_{\rm b}}(z,\hat{\mathbf{n}}) &= \frac{1}{\mathcal{H}}\int \frac{{\rm d}^3\mathbf{k}}{(2\pi)^{3/2}}\tilde{v}(\mathbf{k})\left(\frac{1}{k}\frac{\partial^2}{\partial\chi^2}{\rm e}^{i\mathbf{k}\cdot\mathbf{r}}\right) \\
&= \sum_{\ell m}\left[(4\pi i^\ell)\int \frac{{\rm d}^3\mathbf{k}}{(2\pi)^{3/2}}\left(\frac{1}{\mathcal{H}}\tilde{v}(\mathbf{k}) k j''_\ell(k\chi)\right) Y^*_{\ell m}(\hat{\mathbf{k}})\right] Y_{\ell m}(\hat{\mathbf{n}}) \\
\Rightarrow \Delta^{(2)}_{T_{\rm b},\ell}(z,\mathbf{k}) &= \frac{1}{\mathcal{H}}\tilde{v}(\mathbf{k}) k j''_\ell(k\chi). \qquad (2.81)
\end{aligned}$$

For the third term in Eq. (2.62), the bracket is just a redshift-dependent term, and the spatial dependent is encoded in $\delta\eta$, so from Eq. (2.47) we want to calculate

$$\mathcal{F}(\delta\eta) = \frac{1}{\mathcal{H}(\bar{\eta}_z)}\mathcal{F}\left[\psi_{\rm A} - \psi + \int_{\eta_{\rm A}}^{\bar{\eta}_z}(\dot{\phi}+\dot{\psi})\mathrm{d}\eta' + \hat{\mathbf{n}}\cdot(\mathbf{v}-\mathbf{v}_{\rm oA})\right]. \tag{2.82}$$

Here we throw out the two constant terms, since they only affect the $\ell = 1$ moment. The ψ term is easy, since it is just the $\tilde{\psi}$. For the velocity term, again we have

$$\begin{aligned}\mathcal{F}(\hat{\mathbf{n}}\cdot\mathbf{v}) &= \hat{\mathbf{n}}\cdot\mathbf{v}(\mathbf{k}) = -i(\hat{\mathbf{k}}\cdot\hat{\mathbf{n}})\tilde{v}(\mathbf{k}) \\ \Rightarrow \Delta_{T_{\rm b},\ell}(z,\mathbf{k}) &\sim -\tilde{v}(\mathbf{k})j'_\ell(k\chi).\end{aligned} \tag{2.83}$$

Finally, for the ISW term, we need to use $\mathrm{d}\chi \simeq -\mathrm{d}\eta$ (neglecting higher order perturbation), and also we need to bear in mind that inside the ISW term in Eq. (2.47), the $\phi(\mathbf{r},\eta)$ and $\psi(\mathbf{r},\eta)$ are functions of spatial hyper-surface at each conformal time η. Therefore we have (For the first line $\mathbf{r}'$ means the 3D hyper-surface at conformal time η')

$$\begin{aligned}&\int_{\eta_{\rm A}}^{\bar{\eta}_z}(\dot{\phi}(\mathbf{r}',\eta')+\dot{\psi}(\mathbf{r}',\eta'))\mathrm{d}\eta' \\ &= \int_{\eta_{\rm A}}^{\bar{\eta}_z}\mathrm{d}\eta'\left[\int\frac{\mathrm{d}^3\mathbf{k}}{(2\pi)^{3/2}}(\dot{\tilde{\phi}}(\mathbf{k},\eta')+\dot{\tilde{\psi}}(\mathbf{k},\eta'))\mathrm{e}^{i\mathbf{k}\cdot\mathbf{r}'(z',\hat{\mathbf{n}})}\right] \\ &= \int_{\eta_{\rm A}}^{\bar{\eta}_z}\mathrm{d}\eta'\left[\int\frac{\mathrm{d}^3\mathbf{k}}{(2\pi)^{3/2}}(\dot{\tilde{\phi}}(\mathbf{k},\eta')+\dot{\tilde{\psi}}(\mathbf{k},\eta'))\left(\sum_{\ell m}(4\pi i^\ell)j_\ell(k\chi')Y^*_{\ell m}(\hat{\mathbf{k}})Y_{\ell m}(\hat{\mathbf{n}})\right)\right] \\ &= \sum_{\ell m}\left[(4\pi i^\ell)\int\frac{\mathrm{d}^3\mathbf{k}}{(2\pi)^{3/2}}\left(-\int_0^\chi\mathrm{d}\chi'(\dot{\tilde{\phi}}(\mathbf{k},\eta')+\dot{\tilde{\psi}}(\mathbf{k},\eta'))j_\ell(k\chi')\right)Y^*_{\ell m}(\hat{\mathbf{k}})\right]Y_{\ell m}(\hat{\mathbf{n}}) \\ \Rightarrow \Delta_{T_{\rm b},\ell}(z,\mathbf{k}) &\sim -\int_0^\chi\mathrm{d}\chi'(\dot{\tilde{\phi}}+\dot{\tilde{\psi}})j_\ell(k\chi').\end{aligned} \tag{2.84}$$

Note that j_ℓ function is just to tell how different Fourier modes project onto different angular scales.

Therefore, the third term in Eq. (2.62) all together becomes

$$\Delta^{(3)}_{T_{\rm b},\ell}(z,\mathbf{k}) = -\left(\frac{1}{\mathcal{H}}\frac{\mathrm{d}\ln(a^3\bar{n}_{\rm HI})}{\mathrm{d}\eta} - \frac{\dot{\mathcal{H}}}{\mathcal{H}^2} - 2\right)\times\left[\tilde{\psi}j_\ell(k\chi)+\tilde{v}(\mathbf{k})j'_\ell(k\chi)+\int_0^\chi(\dot{\tilde{\phi}}+\dot{\tilde{\psi}})j_\ell(k\chi')\mathrm{d}\chi'\right] \tag{2.85}$$

Therefore, the whole $\Delta_{T_{\rm b},\ell}(\mathbf{k},z)$ is

$$\begin{aligned}\Delta_{T_{\rm b},\ell}(\mathbf{k},z) &= \Delta^{(1)}_{T_{\rm b},\ell}(\mathbf{k},z)+\Delta^{(2)}_{T_{\rm b},\ell}(\mathbf{k},z)+\Delta^{(3)}_{T_{\rm b},\ell}(\mathbf{k},z)+\Delta^{(4)}_{T_{\rm b},\ell}(\mathbf{k},z)+\Delta^{(5)}_{T_{\rm b},\ell}(\mathbf{k},z) \\ &= \left(\tilde{\delta}_n+\frac{1}{\mathcal{H}}\dot{\tilde{\phi}}+\tilde{\psi}\right)j_\ell(k\chi)+\frac{1}{\mathcal{H}}\tilde{v}(\mathbf{k})kj''_\ell(k\chi) \\ &- \left(\frac{1}{\mathcal{H}}\frac{\mathrm{d}\ln(a^3\bar{n}_{\rm HI})}{\mathrm{d}\eta} - \frac{\dot{\mathcal{H}}}{\mathcal{H}^2} - 2\right)\times\left[\tilde{\psi}j_\ell(k\chi)+\tilde{v}(\mathbf{k})j'_\ell(k\chi)+\int_0^\chi(\dot{\tilde{\phi}}+\dot{\tilde{\psi}})j_\ell(k\chi')\mathrm{d}\chi'\right].\end{aligned} \tag{2.86}$$

The square bracket "$[\times\times\times]$" has clear physical meaning. The first term, second term and third term in the square bracket is just the usual SW, Dopper shift and ISW contributions,

which are the usual contribution from CMB. It has to multiply with the front factor, which is basically $\mathrm{d}\bar{T}_\mathrm{b}/\mathrm{d}\eta$. For the second term, if HI is not moving, and the observer collects photons at a frequency ν, then the observer knows it was emitted at at certain time; if HI is moving, then the observer collects photons at a frequency ν, then the observer knows that it was emitted at earlier or later time. Therefore the signal that the observer collects depends on whether HI is moving or not. This is analogous to the CMB where the photons were emitted at a thin shell at fixed epoch. In brief, the second term arises because emitting gas with peculiar velocity lies at a different comoving distance than the FRW prediction for its observed redshift. So when we observe temperature fluctuations across the sky at fixed redshift, we are observing gas at different conformal distances. The background temperature monopole is hence different too, since it evolves with time, and so the observed fluctuation is given by the time-shift multiplied by the time-derivative of the background, evaluated at the background time corresponding to the observed redshift. This is clearly gauge-dependent as it depends on how events in the perturbed universe are mapped to those in the background, but the sum of all terms is Eq. (2.86) is gauge invariant.

In the first bracket, δ_n is the intrinsic fluctuation. The second v term is the usual redshift-space distortion term. But the $(\dot{\tilde{\phi}}/\mathcal{H} + \tilde{\psi})$ does not have the usual meaning.

The contribution to the large angular part (small ℓ) of angular power spectrum of 21-cm comes from small physical scales (large k-value), also the large angular scale (small ℓ), the power spectrum of 21-cm is almost a constant. To see this, we expand the linear density field into spherical harmonics, and then expands the exponential in Spherical Harmonic/Bessel functions which gives

$$\delta_{\ell m}(z) = 4\pi i^\ell \int \frac{\mathrm{d}^3\mathbf{k}}{(2\pi)^3}\delta(\mathbf{k}, z) j_\ell(k\chi) Y_{\ell m}(\hat{\mathbf{k}}). \tag{2.87}$$

Now squaring this and using the definition of the 3D power spectrum, one can find

$$C_\ell = (4\pi)\int \mathrm{d}\ln k \left(\frac{k^3 P(k)}{2\pi^2}\right) j_\ell(k\chi)^2, \tag{2.88}$$

where the dimensionless power spectrum $k^3P(k)/2\pi^2 \sim k^4$ on large physical scales (here we distinguish angular scale (in ℓ) and physical scales (in k)). Therefore, because $k^3P(k)$ is rising rapidly, most of the contribution to this integral comes from scales having $k \gg \ell/\chi$ when ℓ is small. When is ℓ is of order a few, ℓ/χ is of order the horizon, and horizon-scale power is very small compared to sub-horizon power when dealing with the density field. Therefore we can approximate the Bessel function with its asymptotic form at $\ell \ll k\chi$, which is

$$j_\ell(x) = \frac{1}{x}\sin\left(x - \frac{\ell\pi}{2}\right). \tag{2.89}$$

On the small physical scales relevant for this integral, $k\chi \gg 1$, so this sinusoidal function is rapidly oscillating. Therefore, when we do the integral

$$C_\ell \sim \int \mathrm{d}k k^3 j_\ell^2(k\chi) \sim \int \mathrm{d}k k^3 \frac{1}{(k\chi)^2}\sin^2\left(k\chi - \frac{\ell\pi}{2}\right) = \frac{1}{\chi^2}\int \mathrm{d}k k\left[\frac{1}{2}\left(1 - \cos\left(2k\chi - \ell\pi\right)\right)\right] \tag{2.90}$$

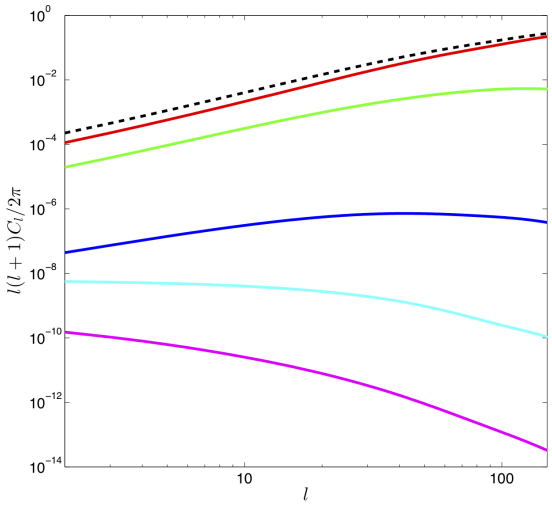

Figure 13: Fractional brightness temperature (dimensionless) perturbation power spectrum at $z = 1$ with a 2 MHz bandwidth. The auto-spectra of the full signal (black dashed line) and of each individual term in Eq. (2.86) are shown, generically grouped (solid lines, top to bottom respectively) as Newtonian-gauge density (red), redshift-space distortions (green), velocity terms (blue), all potential terms evaluated at the source position (cyan) and the ISW term (magenta). Figure taken from [8].

where the rapid oscillation part averaged over a period and left with 1/2, and as the only ℓ-dependence was in the phase of the sine, the ℓ-dependence disappears and we're left $C_\ell =$ constant.

For a simple example which demonstrates this, consider doing the integral

$$\int \mathrm{d}x \sin(ax) * \cos^2(bx), \tag{2.91}$$

if $b \gg a$, this reduces to $-\cos(x)/(2a)$, i.e. half the integral of $\sin(ax)$.

2.2.8 Power spectra and its relative components

Once we obtain the $\Delta_{T_\mathrm{b},\ell}(\mathbf{k}, z)$, we can integrate it over the frequency band and calculate the projected $\Delta_{T_\mathrm{b},\ell}$ for each $\mathbf{k}$ for band W.

$$\Delta_{T_\mathrm{b},\ell}(\mathbf{k}) = \int \mathrm{d}z W(z) \Delta_{T_\mathrm{b},\ell}(\mathbf{k}, z), \tag{2.92}$$

and then we define

$$\Delta'_{T_\mathrm{b},\ell}(k) = \Delta_{T_\mathrm{b},\ell}(\mathbf{k})/\mathcal{R}(\mathbf{k}), \tag{2.93}$$

and power spectrum is

$$C_\ell^{WW'} = 4\pi \int \mathrm{d}\ln k P_\mathcal{R}(k) \Delta'^{W}_{T_\mathrm{b},\ell}(k) \Delta'^{W'}_{T_\mathrm{b},\ell}(k). \tag{2.94}$$

We plot the different components of the relativistic power spectra in Fig. 13 for $z = 1$ and $\Delta\nu = 2$ MHz. The RSD term will drop if one has very large frequency band width, because the radial integral of line-of-sight over many peaks and troughs will turn to be close to zero.

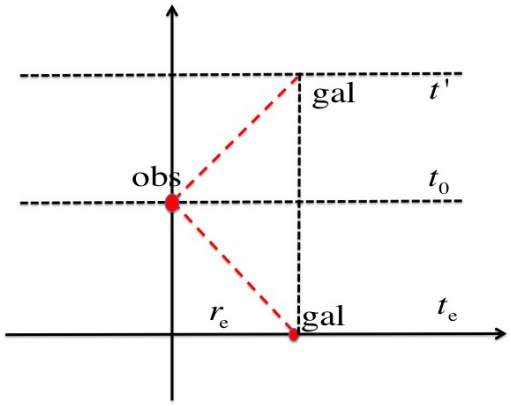

Figure 14: The spacetime diagram for an observer locating at t_0 at spatial coordinate $r = 0$ observing an invariant area (of galaxies) emitting signal at t_e at comoving spatial distance r_e. Also for the same galaxy observing an invariant area emitting a signal at t_0.

3 Observational prospects for 21-cm intensity mapping

Please read the presentation slides for this section.

3.1 BAO reconstruction

3.2 Forecasts for BINGO, FAST and SKA

3.3 Foreground removal technique

3.4 $1/f$ noise

A Etherington's Reciprocity relation

Suppose you place a known object of physical size l at an early time t_e at a place with comoving distance r_e. The observer sees the object through the light bundle shown in the lower red dashed in Fig. 14. The comoving size of the object is l/a_e, where $a_e = 1/(1+z)$. Therefore, the angle subtended by the object at t_e seen by the current day observer is $\theta = (l/a_e)/r_e$, therefore

$$\left(\frac{\mathrm{d}A_s}{\mathrm{d}\Omega_o}\right)^{1/2} = \frac{l}{\theta} = D_A(t_e) = a_e r_e. \tag{A.1}$$

Then we ask a question, what is the solid angle seen by the galaxy if we place the same object at observer's position at time t_0? (upper red dashed line in Fig. 14)

The comoving size of the object now becomes l/a_0, and the angle subtended by the object at t_0 is $\theta' = (l/a_0)/r_e$ (note that the comoving distance has *not* changed), therefore

$$\left(\frac{\mathrm{d}A_o}{\mathrm{d}\Omega_s}\right)^{1/2} = \frac{l}{\theta'} = a_0 r_e = (a_e r_e)(a_0/a_e) = \left(\frac{\mathrm{d}A_s}{\mathrm{d}\Omega_o}\right)^{1/2}(1+z), \tag{A.2}$$

where z is the galaxy's redshift. Therefore we proved the Etherington's *reciprocity relation*, i.e. $\mathrm{d}A_\mathrm{s}\mathrm{d}\Omega_\mathrm{s} = \mathrm{d}A\mathrm{d}\Omega/(1+z)^2$. In the notation of this note, it is $\mathrm{d}\tilde{A}\mathrm{d}\tilde{\Omega} = \mathrm{d}A\mathrm{d}\Omega/(1+z)^2$.

Acknowledgements

I would like to thank the discussion with Anthony Challinor, Alex Hall, Yi-Chao Li, and Xiaodong Xu.

References

[1] X. Fan et al., *Astron. J.*, **132**, 117 (2006)

[2] J. Gunn, & B. Peterson, The Astrophysical Journal, 142, 1633, (1965)

[3] X. Fan et al., ARA& A, 44, 415, (2006)

[4] Cohen, A., Fialkov, A., Barkana, R., & Lotem, M. 2017, Monthly Notices of the Royal Astronomical Society, 472, 1915

[5] Pritchard, J. R., & Loeb, A. 2012, Reports on Progress in Physics, 75, 086901

[6] Pritchard, J., & Loeb, A. 2010, Nature, 468, 772

[7] E. Komatsu et al., 2009, ApJS, 180, 330

[8] A. Hall, C. Bonvin, A. Challinor, 2013, Phys. Rev. D., 87, 064026.

[9] A. Challinor, & A. Lewis, 2011, Phys. Rev. D., 84, 3516

[10] P. Schneider, J. Ehlers, & E. E. Falco, *Gravitational Lenses* (Springer-Verlag, Berlin, 1992)

[11] A. Mesinger, S. Furlanetto, & R. Cen, 2011, MNRAS, 411, 955